How well can we quantify dust deposition to the ocean?

R. F. Anderson, H. Cheng, R. L. Edwards, M. Q. Fleisher, C. T. Hayes, K.-F. Huang, D. Kadko, P. J. Lam, W. M. Landing, Y. Lao, et al.

PHILOSOPHICAL TRANSACTIONS A

rsta.royalsocietypublishing.org

Research

Cite this article: Anderson RF *et al*. 2016 How well can we quantify dust deposition to the ocean? *Phil. Trans. R. Soc. A* **374**: 20150285. http://dx.doi.org/10.1098/rsta.2015.0285

Accepted: 10 August 2016

One contribution of 20 to a discussion meeting issue 'Biological and climatic impacts of ocean trace element chemistry'.

Subject Areas:
oceanography, geochemistry, atmospheric science

Keywords:
dust, aerosols, GEOTRACES, northeast tropical Atlantic

Author for correspondence:
R. F. Anderson
e-mail: boba@ldeo.columbia.edu

How well can we quantify dust deposition to the ocean?

R. F. Anderson[1,2], H. Cheng[3,4], R. L. Edwards[3], M. Q. Fleisher[1], C. T. Hayes[5], K.-F. Huang[6], D. Kadko[7], P. J. Lam[8], W. M. Landing[9], Y. Lao[10], Y. Lu[11], C. I. Measures[12], S. B. Moran[13], P. L. Morton[9], D. C. Ohnemus[14], L. F. Robinson[15] and R. U. Shelley[16]

[1]Lamont-Doherty Earth Observatory, Columbia University, Palisades, NY 10964, USA
[2]Department of Earth and Environmental Sciences, Columbia University, New York, NY 10027 USA
[3]Department of Earth Sciences, University of Minnesota, Minneapolis, MN 55455, USA
[4]Institute of Global Environmental Change, Xi'an Jiaotong University, Xi'an, People's Republic of China
[5]Department of Marine Science, University of Southern Mississippi, Stennis Space Center, MS 39529, USA
[6]Institute of Earth Sciences, Academia Sinica, Taipei, Taiwan, Republic of China
[7]Applied Research Center, Florida International University, Miami, FL 33174, USA
[8]Department of Ocean Sciences, University of California Santa Cruz, Santa Cruz, CA 95064, USA
[9]Department of Earth, Ocean and Atmospheric Science, Florida State University, Tallahassee, FL 32306, USA
[10]Department of Laboratory Services, Massachusetts Water Resources Authority, 190 Tafts Avenue, Winthrop, MA 02152, USA
[11]Earth Observatory of Singapore, 50 Nanyang Avenue, Singapore 639798, Republic of Singapore
[12]Department of Oceanography, University of Hawaii, Honolulu, HI 96822, USA
[13]College of Fisheries and Ocean Sciences, University of Alaska Fairbanks, Fairbanks, AK 99775, USA
[14]Bigelow Laboratory for Ocean Sciences, East Boothbay, ME 04544, USA
[15]School of Earth Sciences, University of Bristol, Queens Road, Bristol BS8 1RJ, UK

THE ROYAL SOCIETY PUBLISHING

[16]LEMAR/UMR CNRS 6539/IUEM, Technopôle Brest-Iroise, Place Nicolas Copernic, Plouzané 29280, France

RFA, 0000-0002-8472-2494

rsta.royalsocietypublishing.org Phil. Trans. R. Soc. A 374: 20150285

Deposition of continental mineral aerosols (dust) in the Eastern Tropical North Atlantic Ocean, between the coast of Africa and the Mid-Atlantic Ridge, was estimated using several strategies based on the measurement of aerosols, trace metals dissolved in seawater, particulate material filtered from the water column, particles collected by sediment traps and sediments. Most of the data used in this synthesis involve samples collected during US GEOTRACES expeditions in 2010 and 2011, although some results from the literature are also used. Dust deposition generated by a global model serves as a reference against which the results from each observational strategy are compared. Observation-based dust fluxes disagree with one another by as much as two orders of magnitude, although most of the methods produce results that are consistent with the reference model to within a factor of 5. The large range of estimates indicates that further work is needed to reduce uncertainties associated with each method before it can be applied routinely to map dust deposition to the ocean. Calculated dust deposition using observational strategies thought to have the smallest uncertainties is lower than the reference model by a factor of 2–5, suggesting that the model may overestimate dust deposition in our study area.

This article is part of the themed issue 'Biological and climatic impacts of ocean trace element chemistry'.

1. Introduction

Efforts to evaluate the supply of dust to the ocean are motivated in large part by the desire to assess the role of aerosols as a source of iron, an essential nutrient whose abundance is thought to influence rates and geographical patterns of photosynthesis and nitrogen fixation [1–7]. Ocean productivity, in turn, is a major component of the global carbon cycle [8], so there is a recognized need to include dust supply in global biogeochemical models [9].

As dissolved Fe is highly insoluble in seawater [10], it is removed by abiotic scavenging processes as well as by biological uptake [11]. When nutrients regenerated from biogenic material are supplied to the euphotic zone by mixing from below, they are often deficient in Fe relative to nitrogen and phosphorus [12] because Fe is lost via scavenging. Under these conditions, the availability of Fe in surface waters may depend on external sources, among which continental mineral aerosols (dust) represent the dominant supply mechanism in many regions [13–16].

A variety of techniques have been used to assess dust deposition to the ocean. Each has its strengths and weaknesses. Difficulties arise from the need to extrapolate the measured signal to a rate of deposition and also from the different time scales over which the measurements integrate. For example, direct collection of atmospheric aerosols is the most straightforward approach (e.g. [17]) but this strategy is limited by the availability of an appropriate location (e.g. an island placement) or, if on a ship, by the limited time that aerosols can be collected in any given place during a cruise. A significant source of uncertainty for this method involves turning measured aerosol loads into deposition by applying a settling velocity, which can vary by a factor of 3 [18].

Owing to the paucity and difficulty of observations, it is generally necessary to rely on model estimates of dust deposition to assess its impact on marine ecosystems and biogeochemical cycles [2,19]. A number of different approaches have been employed to assess the accuracy of dust models, revealing substantial inconsistencies in dust emission, horizontal and vertical distribution of dust, atmospheric lifetime and dust deposition, both among models and between models and observations [17,19–24]. These uncertainties limit the use of dust models in assessing the impact of dust on marine ecosystems. Most models reproduce dust deposition within an order of magnitude of fluxes measured at point locations, although agreement is poorer for surface

aerosol concentration. Model–data agreement is generally better for sites immediately downwind of major dust sources (e.g. NW Africa [19,21]).

Satellite (e.g. [20,23,25]) and ground-based (AERONET; AErosol RObotic NETwork, http://aeronet.gsfc.nasa.gov) products for aerosol optical properties provide valuable resources for evaluating and improving model performance because of their near-global coverage. However, dust deposition is not necessarily correlated with optical properties [19], so previous studies have recommended expanded efforts to measure dust deposition to assess and improve the ability of models to simulate dust deposition [2,17,19–21,25,26].

Geochemical methods to estimate dust deposition use indirect chemical signals in the ocean water column and sediments. Some of these approaches rely on assumptions about aerosol solubility, which varies significantly in time and space, as well as on estimates of the tracer's residence time in the water column, which varies with primary production (discussed in §3). A further problem of these approaches for tracers with longer residence times is that currents can advect surface waters considerable distances during the integration period of the tracer, smearing the aerosol deposition signal across hydrographic regimes. Estimates of lithogenic material fluxes from sediment traps [27] suffer from the well-documented over- and under-collection problems in both the near-surface and near-bottom regions of the water column, while accumulation of lithogenic material within surface sediments [27,28] is subject to bias from sediment resuspension processes (turbidity currents, nepheloid layers, etc.) and also integrates over time scales of hundreds to thousands of years.

Many of the variables used in these geochemical strategies are measured systematically as part of the GEOTRACES global survey, an international study of the marine biogeochemical cycles of trace elements and their isotopes (www.geotraces.org, [29,30]). Although these approaches are based on established geochemical principles, there has until now been no systematic intercomparison of results obtained by the various approaches. If these approaches could be shown to be reliable, then their widespread application in GEOTRACES would represent a valuable asset to quantify the supply of dust and essential nutrients. These techniques would also complement satellite and ground-based measurements as benchmarks for assessing model performance. Unfortunately, there is no absolute reference against which to assess the accuracy of any method to evaluate dust deposition. Consequently, here we take an intermediate step in working towards reliable dust fluxes by examining the internal consistency among methods based on ocean observations within a specific region downwind from North Africa.

2. Study area and general strategy

The Eastern Tropical North Atlantic Ocean (ETNA), downwind from North Africa, experiences among the highest dust deposition in the global ocean [19,31]. Investigators participating in the US contribution to the GEOTRACES programme sampled a number of dust-relevant variables along a track (GA03) within the region of maximum expected dust deposition (figure 1).

Transport of dust from North Africa across the ETNA is highly seasonal, peaking in boreal summer [25]. However, in summer, dust is transported out of Africa primarily at high altitude [25], eventually reaching the Americas [17,32] without depositing a large amount of dust in the ETNA. By contrast, maximum surface dust concentration at the Cape Verde Islands [33] and maximum dust deposition in the ETNA [34,35] occur during boreal winter (December, January, February), reflecting dust transport by low-level Saharan air masses. GA03 stations used in this study (figure 1) were occupied in November 2010 (four stations, Africa to the Cape Verde Islands, KN199-4) and in December 2011 (five stations, Mid-Atlantic Ridge (MAR) to Cape Verde, KN204-1) [36], early in the seasonal period of maximum dust deposition.

3. Methods and results

We examine a variety of approaches to evaluate dust deposition to the ETNA, using data collected primarily during the GEOTRACES expeditions and supplemented with published

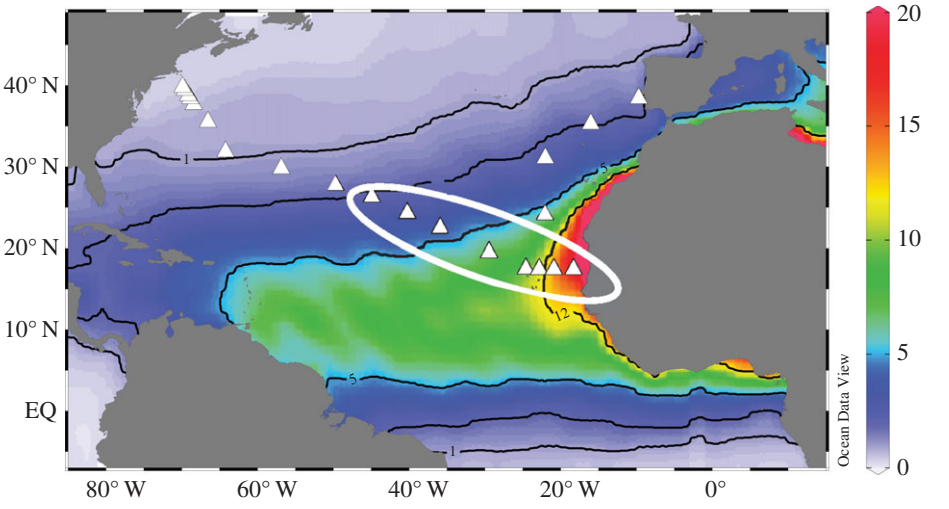

Figure 1. Base map illustrates mean annual deposition of desert dust (g m^{-2} yr^{-1}) extracted from the model of Mahowald *et al.* [31] used here as a reference. Triangles indicate full-depth stations occupied during the US GEOTRACES expeditions that sampled on a section designated as GA03 in 2010 and in 2011 (http://www.bodc.ac.uk/geotraces/cruises/section_maps/atlantic_ocean/). The white oval outlines the stations that are used in this study, covering a large gradient in modelled dust deposition between the coast of Africa and the Mid-Atlantic Ridge (roughly 45° W). Nine hydrographic stations, at eight locations, are used for this study. The station at 24.5° W was occupied during both expeditions.

results. We provide only a brief description of each observational approach to quantify dust deposition; additional details are contained in the cited literature. Specific sources of uncertainty are discussed as each method is introduced in §3. A more general discussion and assessment of uncertainties are presented in §4.

Each set of observational estimates is compared with the mean annual deposition of desert dust simulated by the model of Mahowald *et al.* [31] at the coordinates of the hydrographic stations (figure 1). The use of this model, or any other, implies no judgement concerning its accuracy. It provides a benchmark against which we can compare the estimates derived from the suite of observational strategies.

(a) Aerosol deposition

Aerosols were collected during the GA03 expeditions on 12 replicate acid-washed 47 mm diameter Whatman 41 filters at a total flow rate of approximately 1.3 m^3 min^{-1} [37]. Samplers were deployed on the ship's flying bridge and samples were collected only when the wind was ±60° from the bow and more than 0.5 m s^{-1}. Procedures for filter digestion and for the analysis of a suite of major and trace elements by inductively coupled plasma mass spectrometry are described by Shelley *et al.* [37].

Adopting the approach of Shelley *et al.* [37], we estimate dust deposition from measured aerosol Al concentrations by assuming an average upper continental crust (UCC) value of 8% Al [38] in Saharan dust. Shelley *et al.* noted that Saharan dust is measurably depleted in Al relative to UCC, but any error introduced by assuming a UCC value would be small compared with other sources of uncertainty.

Continuing to follow the approach of Shelley *et al.* [37], we adopt an average dust bulk settling velocity of 1000 m day^{-1}. In areas where wet deposition delivers most of the dust, it may be inappropriate to use an average aerosol settling velocity. However, dry deposition dominates the total dust deposition our study area in the ETNA north of the region influenced by the Intertropical Convergence Zone [34,35]. Aerosol settling velocity depends on particle size, wind speed, relative humidity, air viscosity and sea surface roughness [18]. Duce *et al.* [18] recommend

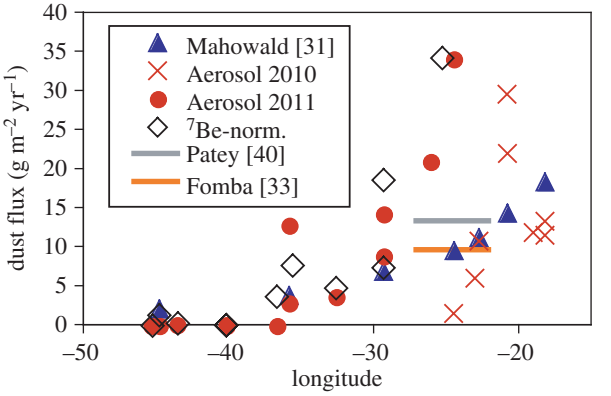

Figure 2. Dust deposition in the Eastern Tropical North Atlantic Ocean estimated from surface aerosol concentrations. Red crosses and filled circles represent dust deposition calculated from shipboard surface aerosol Al concentrations measured in 2010 and 2011, respectively, assuming an average settling rate of 1000 m day^{-1} [37]. Open diamonds indicate the dust deposition calculated using the surface aerosol Al concentration normalized to the ^{7}Be concentration measured in the same samples (available only for the 2011 expedition). Grey line is the dust deposition calculated from the average (July 2007–July 2008) aerosol Al concentration measured at the Cape Verde Atmospheric Observatory (CVAO, 16.87° N, 24.87° W [40]) assuming 8% Al in dust and an aerosol settling velocity of 1000 m day^{-1}. Tan line is the dust deposition calculated from the 5-year average (2007–2011) aerosol dust concentration measured at the CVAO [33] assuming an aerosol settling velocity of 1000 m day^{-1}. Blue triangles represent annual average desert dust deposition from the reference model of Mahowald *et al.* [31].

an average settling velocity of 1.0 cm s^{-1} (± a factor of 3) for particle sizes more than 1.0 µm. Given that the typical size distribution of dust in the ETNA falls above 1 µm [39], a slightly larger settling velocity (1000 m day^{-1} corresponds to 1.2 cm s^{-1}) is appropriate.

Dust deposition is highly episodic. In many areas, a large fraction of the annual dust deposition occurs within a period of only a few days [17,19], reflecting short-term variability of meteorological conditions that influence dust mobilization, transport and deposition. This principle is well illustrated by the two occupations of the station at 24.5° W, which produce the highest (2011, red circle) and lowest (2010, red cross) estimates of dust flux in the eastern half of our study area (figure 2). Consequently, the observed sample-to-sample variability in the calculated dust deposition is to be expected. Nevertheless, the average trend of aerosol data (red symbols in figure 2) roughly follows the pattern (blue triangles) generated by the model of Mahowald *et al.* [31].

For further comparison, we include dust deposition estimated by applying a bulk aerosol settling velocity of 1000 m day^{-1} to annual average aerosol concentrations available from time-series records at the Cape Verde Atmospheric Observatory (16.87° N, 24.87° W). Dust deposition is calculated to be 9.5 g m^{-2} yr^{-1} using the 5-year (2007–2011) average aerosol dust concentration of Fomba *et al.* [33] and 13.2 g m^{-2} yr^{-1} using the average aerosol Al concentration reported by Patey *et al.* [40] for the period July 2007–July 2008, assuming 8% Al in the dust (figure 2). The larger dust deposition estimated for 2007–2008 reflects the greater aerosol concentrations during that year compared to the full 5-year record [33]. These estimates are consistent with dust deposition in this region in the reference model (figure 2).

(b) ^{7}Be-normalized flux

Building on the work of Young & Silker [41], Kadko *et al.* [42] introduced a novel strategy to constrain bulk aerosol settling velocity using the naturally occurring short-lived (half-life 53.3 days) radionuclide ^{7}Be. Beryllium-7 is a spallation product of the interaction of cosmic rays with nitrogen and oxygen in the atmosphere. Once delivered to the ocean, ^{7}Be is relatively conservative, with an average residence time for dissolved Be of about 1000 years [43], meaning

that its distribution in the upper ocean reflects a balance between atmospheric deposition, radioactive decay and physical transport [44].

Concentrations of ^{7}Be on aerosol samples collected during the 2011 GA03 expedition were measured following methods described in Kadko *et al.* [42]. Water-column inventories of ^{7}Be along the GA03 track were estimated by eye from figure 6 of Young & Silker [41], which presents a climatology of the inventory of ^{7}Be in the upper ocean of the Northern Hemisphere. For each aerosol sample, an average bulk settling velocity (S_A, m day^{-1}) was calculated as

$$S_A = \lambda_{Be} \cdot \frac{I_{Be}}{C_{Be}}, \tag{3.1}$$

where λ_{Be} is the radioactive decay constant of ^{7}Be (0.013 day^{-1}), I_{Be} is the inventory of dissolved ^{7}Be in the water column (dpm m^{-2}) and C_{Be} is the measured concentration of ^{7}Be in aerosols (dpm m^{-3}) (dpm = disintegrations per minute). The aerosol bulk settling velocity for each sample was then multiplied by the aerosol Al concentration in the corresponding sample to derive dust deposition, assuming 8% Al in the dust, as above. Dust fluxes estimated by normalizing to ^{7}Be are generally consistent with those derived assuming a uniform settling rate of 1000 m day^{-1} and with the reference model (figure 2).

Baker *et al.* [45] emphasize the need to use the full equation (not shown here) for bulk (wet plus dry) aerosol deposition. They also point out that ^{7}Be is preferentially incorporated into fine aerosols and removed by wet deposition, which may require adjustments to the bulk deposition equation in areas where wet deposition is significant. The consistency of the fluxes obtained in our study by normalizing to ^{7}Be with those estimated using an average settling velocity of 1000 m day^{-1} (figure 2) may reflect the dominance of aerosol flux by dry deposition in our study area (§3a).

(c) Surface-ocean dissolved Al inventory and aerosol Al solubility

Throughout much of the open ocean, dust is the principal source of dissolved trace elements in surface waters [14]. Measures & Brown [46] noted that, in regions where dust is the principal source of dissolved Al, such as the ETNA, and assuming steady state, the deposition of dust (F_D) can be derived from the measured inventory of dissolved Al in the mixed layer (I_{Al}) if the Al content of dust (D_{Al}), the fraction of dust-derived Al that dissolves in seawater (Sol_{Al}) and the residence time of dissolved Al in the mixed layer (τ_{Al}) are known. The relationship is

$$F_D = \frac{I_{Al}}{D_{Al} \cdot Sol_{Al} \cdot \tau_{Al}}. \tag{3.2}$$

Dust fluxes derived using this approach are generally consistent with estimates based on other methods [13,46–49]. The inventory of dissolved Al was measured along GA03 [50], and the Al content of continental mineral aerosols does not vary much from the UCC value of 8%, so the principal sources of uncertainty associated with this approach involve Sol_{Al} and τ_{Al}, each of which may vary in time and space. For example, reported values of Sol_{Al} vary by more than an order of magnitude, generally decreasing with increasing aerosol concentration [51,52]. Similarly, τ_{Al} may be as much as an order of magnitude lower in biologically productive upwelling regimes than in the oligotrophic central ocean gyres due to the greater intensity of scavenging and removal of dissolved Al in particle-rich environments [53].

A further complication is that Sol_{Al} is operationally defined and results are highly method-dependent. For example, applying a sequential leach method to the aerosol samples used in this study, Shelley *et al.* [54] found the Sol_{Al} obtained using the acetic acid (pH 2) hydroxylamine hydrochloride ('acetate') leach of Berger *et al.* [55] to be about an order of magnitude greater than for the same samples using the instantaneous deionized water ('DI') leach of Buck *et al.* [56]. For the stations between Africa and the Cape Verde Islands, Sol_{Al} obtained using the acetate leach averaged about 10% while Sol_{Al} determined using the DI leach varied between 0.3% and 1.0%. As expected, measured values of Sol_{Al} with both leaching procedures increased westwards,

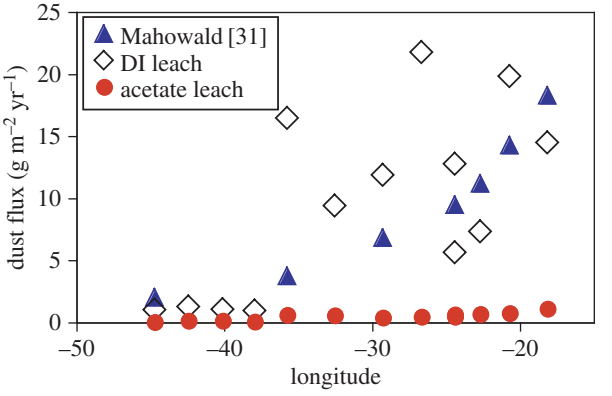

Figure 3. Dust deposition in the Eastern Tropical North Atlantic calculated (equation (3.2)) following the approach of Measures & Brown [46] using measured dissolved Al inventories in the upper 50 m [50] and estimates of aerosol Al solubility based on the instantaneous deionized water leach (DI, [56]) and the acetate-reducing agent leach (acetate, [55]). A residence time for dissolved Al in the upper ocean of 5 years was assumed for all stations. Model results of Mahowald *et al.* [31] are shown for reference (blue triangles).

consistent with decreasing aerosol concentrations. Measures *et al.* [50] estimated dust deposition using equation (3.2) for the entire GA03 track assuming a constant Sol_{Al} of 3%, a value that falls between the two sets of measured Sol_{Al} results for the easternmost stations under the influence of Saharan air masses, but below the Sol_{Al} measured by both methods at central Atlantic stations influenced by low-aerosol marine air masses [37].

We derive estimates of dust deposition (figure 3) based on the measured dissolved Al inventory in the upper 50 m at each GA03 station [50] using the two sets of measured Sol_{Al} values (acetate and DI) and an assumed τ_{Al} of 5 years, the value used by Measures *et al.* [50]. Aerosol sampling often occurs while the ship is under way, so the locations of the aerosol samples used here to constrain Sol_{Al} do not correspond precisely to the locations of the hydrographic stations at which dissolved Al concentrations were measured. For each hydrographic station, we used the aerosol leach results for filters collected nearest to the station. In some cases, results from more than one aerosol sample were averaged.

Taken at face value, the DI leaches produce dust deposition in better agreement with the model of Mahowald *et al.* [31] than the more aggressive acetate leach (figure 3). However, as noted above, τ_{Al} may be as much as an order of magnitude less than the assumed value of 5 years in regions of abundant particles [53], such as the biologically productive Canary Current upwelling regime in the eastern portion of our study area [57]. Furthermore, dilution of Al in the surface layer by upwelling of Al-depleted thermocline water off NW Africa (see fig. 4a in [50]) may add a loss term that is not included in the simple mass balance for dissolved Al [46], thereby introducing a low bias into the derived dust fluxes. When these two factors are taken into account, dust deposition derived using the acetate leach would move towards the reference model and results from the DI leach would be much greater. Improved estimates for τ_{Al} may lead to the conclusion that the acetate leach provides a more representative estimate of aerosol Al solubility than the DI leach.

(d) Surface-ocean dissolved Th inventory and aerosol Th solubility

The approach described in the preceding section can be applied to any trace element for which the inventory in surface water is supplied predominantly by dust. In this context, thorium has an advantage because one isotope (^{232}Th) is supplied by dust, much as for Al, Fe and other trace elements, while other isotopes (^{234}Th, ^{230}Th) are produced uniformly throughout the ocean by radioactive decay of dissolved uranium (^{238}U and ^{234}U, respectively). Assuming steady state, the residence time of dissolved Th calculated from radioactive disequilibrium (^{238}U–^{234}Th or

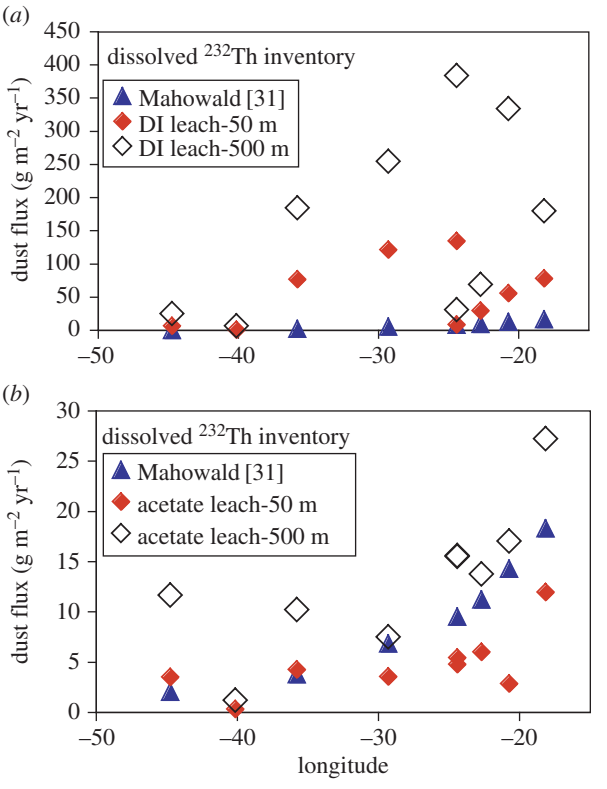

Figure 4. Dust deposition in the Eastern Tropical North Atlantic calculated (equation (3.3)) using measured dissolved ^{232}Th inventories and estimates of aerosol Th solubility based on (*a*) the instantaneous deionized water leach (DI, [56]) and (*b*) the acetate-reducing agent leach (acetate, [55]). In each case, the residence time of Th is derived from the ^{234}U–^{230}Th radioactive disequilibrium integrated from the surface to the depth to which the ^{232}Th inventory is integrated (either 50 m or 500 m). Note the scale change for the ordinate. Model results of Mahowald *et al.* [31] are shown for reference (blue triangles).

^{234}U–^{230}Th) can then be used to establish the rate of supply and removal of dissolved ^{232}Th, provided that the chemical speciation and residence time of each dissolved Th isotope is insensitive to its supply process. If these conditions apply, then dust deposition can be calculated for ^{232}Th, as for Al, using the relationship

$$F_{\mathrm{D}} = \frac{I_{\mathrm{Th}}}{D_{\mathrm{Th}} \cdot \mathrm{Sol}_{\mathrm{Th}} \cdot \tau_{\mathrm{Th}}}. \tag{3.3}$$

This approach, originally proposed by Hirose & Sugimura [58], has been applied in the Atlantic and Pacific Oceans [59–62].

This approach presents a particularity in that the calculated value of dust deposition generally increases with the depth below the sea surface to which dissolved ^{232}Th inventory and ^{230}Th residence time are integrated, levelling off below approximately 500 m [60,61]. The factor(s) responsible for this behaviour are still under study. At present, some investigators derive dust deposition by integrating ^{232}Th inventory and ^{230}Th residence time to 500 m [60,61] whereas others restrict their integration to the mixed layer [59,62].

Furthermore, as for Al, the solubility of aerosol Th in seawater is operationally defined. The acetic acid leach (described above) yields $\mathrm{Sol}_{\mathrm{Th}}$ at our easternmost stations (4–8%) approximately an order of magnitude larger than the DI leach [54]. As there is as yet no preferred method, here we show dust fluxes calculated using $\mathrm{Sol}_{\mathrm{Th}}$ results for both DI and acetate leach and for integration depths of 500 and 50 m (figure 4). As for Al, at each hydrographic station where dissolved Th concentrations were measured, we use $\mathrm{Sol}_{\mathrm{Th}}$ results for the nearest aerosol samples, sometimes averaging results from more than one sample.

In contrast with Al, where dust deposition calculated with DI solubility agreed better with the reference model (figure 3), dust fluxes calculated using Sol_{Th} obtained with the DI method are one to two orders of magnitude greater than the model results (figure 4*a*). Dust deposition calculated using Sol_{Th} obtained with the acetate leach is closer to the model results (figure 4*b*). Neither integration depth produces a systematically better fit to the model across all of the stations. The derived value of dust deposition is more sensitive to the method used to determine Sol_{Th} (average difference between methods is a factor of 13) than to the integration depth (average difference a factor of 3).

(e) Water-column particle settling rate

Multiple strategies to estimate dust deposition, described here and in the following sections, take advantage of the well-constrained mass budget for ^{230}Th in the ocean. These approaches are applied to lithogenic phases in the water column and in the underlying sediments, so they are insensitive to the uncertainty in Sol_{Th} discussed in the previous section.

Radioactive decay of dissolved ^{234}U provides a precisely known source of dissolved ^{230}Th that is uniformly distributed throughout the ocean, varying only with salinity. Dissolved ^{230}Th is removed from the ocean by reversible scavenging to settling particles [63] with a residence time that is sufficiently short (20–40 years in the deep sea) that the tracer experiences relatively little net lateral redistribution between its production in the water column and its burial in the underlying sediments. One modelling study concluded that the removal flux of ^{230}Th to the sediments is within ±30% of its production rate in the overlying water column throughout approximately 70% of the ocean [64], a finding subsequently shown to apply in our study area [65]. Consequently, the short residence time of dissolved Th allows its mass budget to be applied in a one-dimensional framework with relatively small uncertainty.

Profiles of particulate ^{230}Th concentration measured using samples from GA03 [66] collected by *in situ* filtration [67,68] thus offer a novel approach to estimate dust flux. Given the simple mass budget for ^{230}Th in the ocean, where production of dissolved ^{230}Th by ^{234}U decay (P_{Th}, 433 µBq m^{-3} yr^{-1}) is balanced by scavenging loss onto settling particles, one expects the concentration of unsupported (i.e. adsorbed from seawater rather than produced by radioactive decay of U contained within the particle) particulate ^{230}Th, expressed as $C_P(xs^{230}Th)$, to increase linearly with depth (z) according to the relationship

$$\frac{\partial C_P(xs^{230}Th)}{\partial z} = \frac{P_{Th}}{S_P}, \tag{3.4}$$

where S_P is the average settling rate of particles [69]. Although large rare aggregates sink rapidly through the water column [70], there is continuous exchange of material between particle size classes through aggregation and disaggregation [71]. Furthermore, most of the particle mass occurs in smaller size classes. Consequently, here we use the measured ^{230}Th concentrations in the 0.8–51 µm particle size class [66] to derive S_P.

Concentrations of particulate ^{230}Th increase with depth, approximately following the expected linear trend (figure 5*a–e*). Taking the regression slope, $\partial C_P(xs^{230}Th)/\partial z$ (illustrated in figure 5*a–e* for five of our nine stations), we calculate (equation (3.4)) an average particle settling rate for each station. As in previous studies using this approach [69], we find settling velocities in the range of 660–990 m yr^{-1} among the nine stations included in our study (figure 5*f*).

Dust is the primary source of lithogenic particles in the water column of our study area for the portion of the water column unaffected by resuspended sediments [68], so one can use the concentration of any particulate lithogenic element, such as Al or ^{232}Th, to calculate dust flux from the particle settling rate. Here, we calculate dust flux as

$$F_D = C_P(^{232}Th) \cdot \frac{S_P}{D_{Th}}, \tag{3.5}$$

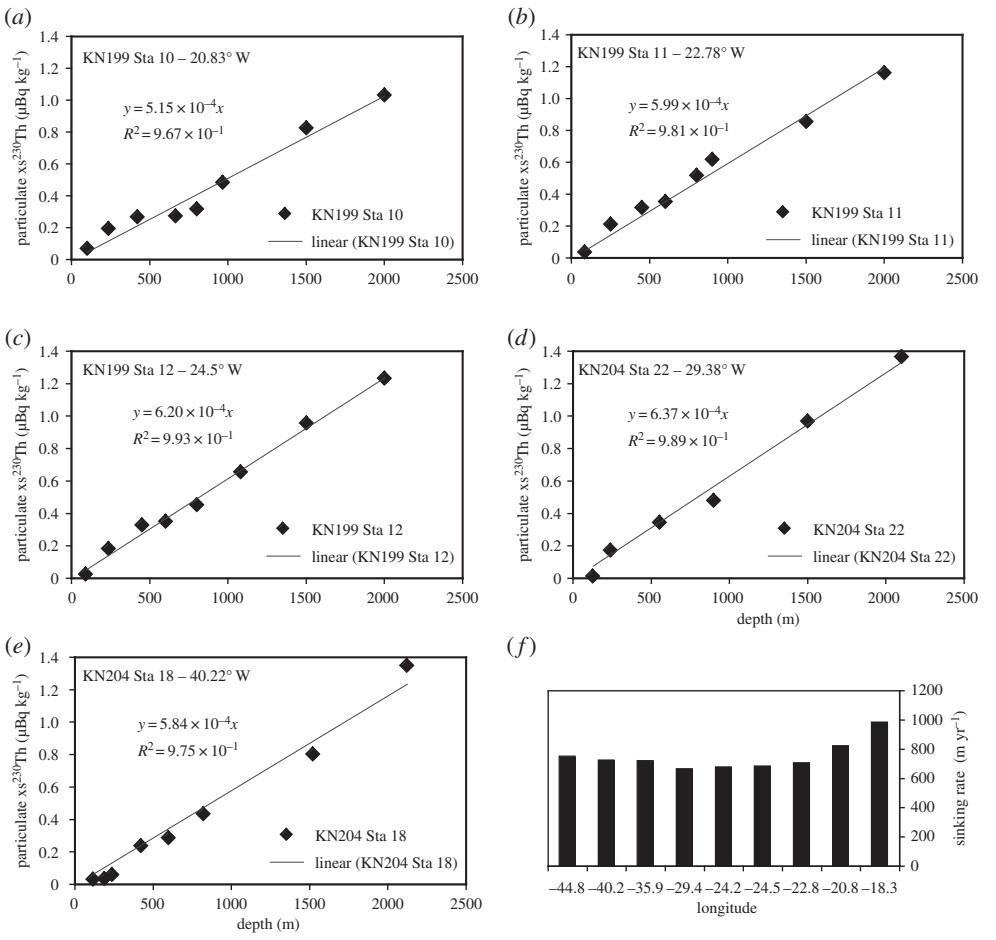

Figure 5. (*a–e*) Concentration profiles of particulate ^{230}Th, $C_P(^{230}Th)$, from Hayes *et al.* [66] at five of the nine hydrographic stations along GA03 used in this study. (*f*) Average particle settling rate at each of the nine hydrographic stations calculated from the slope of each profile (equation (3.4)), as illustrated in panels (*a–e*). Each station in panel (*f*) is plotted at its longitude.

where $C_P(^{232}Th)$ is the particulate ^{232}Th concentration (μg m^{-3}) in the 0.8–51 μm particle size fraction averaged over a depth interval of 235–2100 m (the actual depths of the shallowest and deepest sample vary slightly from station to station), S_P is the average particle settling velocity for each station (figure 5*f*) and D_{Th} is the ^{232}Th content of Saharan dust (13 ppm) [72]. Dust fluxes derived using this approach are lower than those from the model of Mahowald *et al.* [31]. The difference is about a factor of 5–6 at the easternmost stations, decreasing to a factor of 3–4 at the western stations (figure 6*a*).

(f) ^{230}Th-normalized fluxes applied to particles in the water column

A more commonly used strategy that relies on the well-constrained mass budget of ^{230}Th is referred to as ^{230}Th normalization [73]. This approach is widely applied to evaluate the preserved flux of sedimentary constituents, including dust [28,74], while correcting for syndepositional redistribution of sediments by bottom currents. The preserved flux of constituent '*i*' in the sediment is evaluated as

$$F(i) = C(i) \cdot P_{Th} \cdot \frac{z}{C(xs^{230}Th_0)}, \tag{3.6}$$

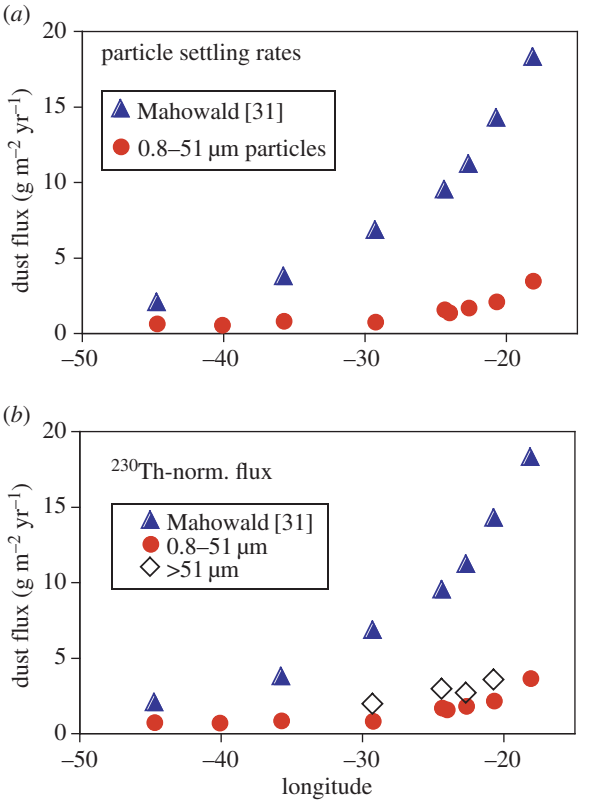

Figure 6. (*a*) Dust deposition in the Eastern Tropical North Atlantic calculated (equation (3.5)) using measured particulate ^{232}Th concentrations in the 0.8–51 µm size fraction, averaged over a depth range of 235–2100 m, multiplied by the average particle settling rate shown in figure 5*f*. In making these calculations it was assumed that all lithogenic material in these samples is derived from dust, and that dust has a ^{232}Th content of 13 ppm [72]. (*b*) Dust deposition in the Eastern Tropical North Atlantic calculated using the ^{230}Th-normalization strategy (equation (3.7)) for the 0.8–51 µm particle size class (red circles, range 0.8 to 3.8 g m^{-2} yr^{-1}) and the more than 51 µm particle size class (open diamonds, range 2.0–3.6 g m^{-2} yr^{-1}) of particles collected by *in situ* filtration. Fluxes plotted here represent averages of all values for each station within the depth range 900–3000 m (figure 7 and see the text). In both (*a*) and (*b*) the difference between observations and the reference model [31] decreases from about a factor of 5 in the east to about a factor of 3 near the Mid-Atlantic Ridge.

where P_{Th} is the production rate of ^{230}Th in the water column, z is the total water depth, $C(i)$ is the concentration of constituent 'i' in the sediment and $C(\mathrm{xs}^{230}\mathrm{Th}_0)$ is the concentration of unsupported ^{230}Th decay corrected to the time of sediment deposition.

This approach can also be applied to particles collected by *in situ* filtration, the method used to collect the samples analysed for this study [67,68]. Particles convey scavenged Th to the sediments, so the amount of adsorbed ^{230}Th on particles filtered from a given depth reflects the integrated production of dissolved ^{230}Th in the overlying water column. Here, we use the same data (concentrations of particulate ^{230}Th and ^{232}Th) as in the previous section. However, with this approach we derive an estimated settling flux of lithogenic particles for each sample rather than an average flux for each station. Substituting ^{232}Th for 'i' in equation (3.6) we have

$$F_{\mathrm{D}} = C(^{232}\mathrm{Th}) \cdot P_{\mathrm{Th}} \cdot \frac{z}{C(\mathrm{xs}^{230}\mathrm{Th}) \cdot D_{\mathrm{Th}}}. \tag{3.7}$$

In contrast with equation (3.6), which is applied to sediments, here C is the measured concentration at the depth (z) at which each particulate sample was collected, so correction for decay is no longer necessary. As for the previous case, we assume 13 ppm ^{232}Th in the lithogenic phases (D_{Th}, [72]).

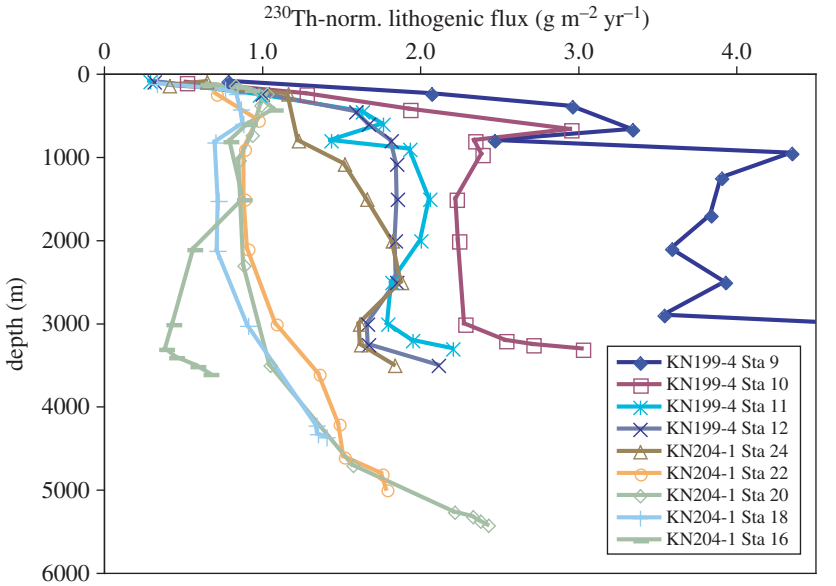

Figure 7. ^{230}Th-normalized settling fluxes of lithogenic material calculated (equation (3.7)) for individual samples of the 0.8–51 µm size fraction of particulate material from the nine stations of GA03 included in this study. Fluxes were estimated using the measured concentration of particulate ^{232}Th and assuming 13 ppm ^{232}Th in the lithogenic material [72]. Station identifications listed in the legend are arranged from east (KN199-Sta 9) to west (KN204-1 Sta 16). KN204-1 Sta 24 is a reoccupation of KN199-4 Sta 12. Average fluxes in the depth interval 900 to 3000 m are presented in figure 6*b*.

This approach is not independent of that used in the preceding section. Rearranging a discretized form of equation (3.4) and substituting for S_P in equation (3.5), and further assuming that $C(\mathrm{xs}^{230}\mathrm{Th}) = 0$ at $z = 0$, leads to equation (3.7). We present the two approaches because each offers advantages under certain conditions. Calculating an average particle settling rate (§3e) has the advantage that it averages out short-term and small-scale variability of particulate ^{232}Th concentrations. The advantage of the approach defined by equation (3.7) is that it can be applied where sampling density is too sparse to derive a good statistical fit to the particulate data. This will be illustrated below when dust fluxes are estimated by applying equation (3.7) to a small number of 'large' (more than 51 µm) particle size fraction samples analysed for this study.

^{230}Th-normalized settling fluxes of lithogenic material, assumed to be derived entirely from dust, tend to increase with depth in the upper approximately 500 m at each of our stations (figure 7). The factors responsible for the apparent flux gradients in the upper water column remain a topic of investigation. One hypothesis is that the trend in the upper 500 m reflects fragmentation in the thermocline of large aggregates that rapidly remove dust grains from the surface mixed layer [68].

The ^{230}Th-normalized flux of lithogenic particles is relatively constant between approximately 1000 and 3000 m at each station (figure 7). Below approximately 3000 m, at some stations, the lithogenic flux again increases with depth, generally at sites where profiles of beam transmission indicate the presence of resuspended sediments [65]. Consequently, here we use the average lithogenic flux between 900 and 3000 m for each station to represent the flux of dust derived using this strategy (figure 6*b*, red circles).

As noted above, large rare aggregates settle much more rapidly than the bulk of the suspended particulate material. Settling rates can be as high as 200–300 m day^{-1} [70]. A few samples of the greater than 51 µm particle size class collected at the GA03 stations [67,68] were also analysed for Th isotopes to investigate the sensitivity of the inferred dust flux to particle size. Only a small percentage of the total collection of greater than 51 µm particle samples could be analysed for Th because it was necessary to process an entire sample to measure Th with good precision,

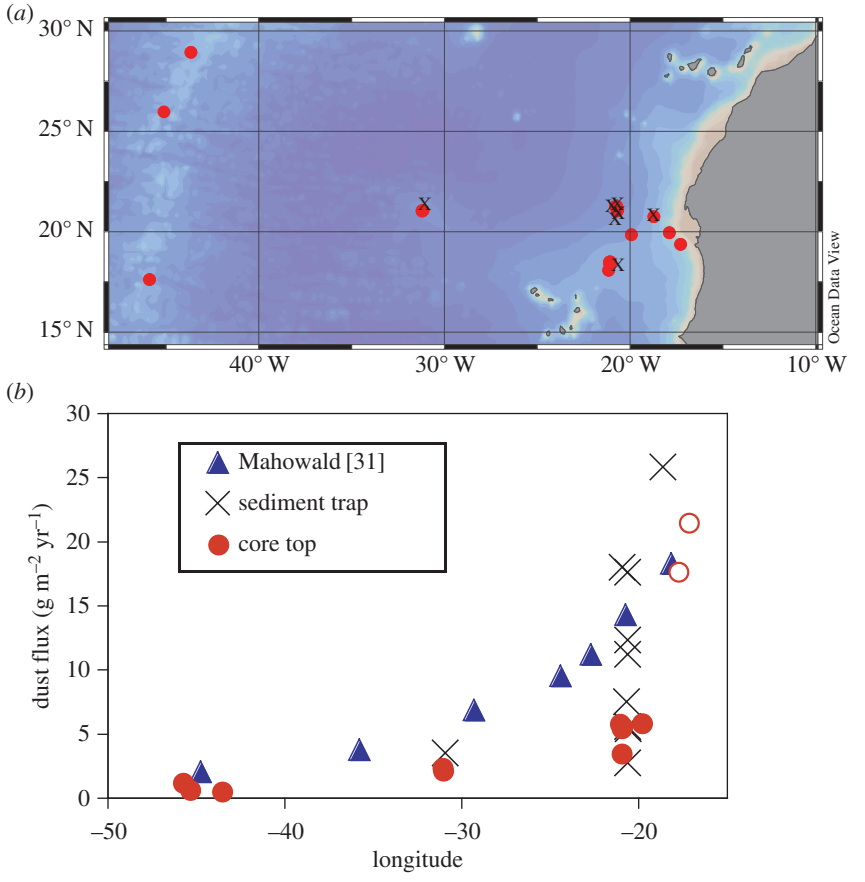

Figure 8. (*a*) Locations of sediment trap moorings (black crosses) for which published annual fluxes of lithogenic material have been compiled (see the text for references), and locations of sediment samples for which ^{230}Th-normalized lithogenic fluxes (red circles) are used to estimate dust deposition. Some sample sites are at the same location, so the symbols lie on top of one another. (*b*) Dust deposition in the Eastern Tropical North Atlantic. Results from sediment traps are shown as crosses and results from sediment cores are indicated by red circles. Open circles in (*b*) are locations where McGee *et al.* [82] used an algorithm based on grain size to distinguish between hemipelagic sources and dust. Only the dust flux is shown. For other sites (solid red circles), the total lithogenic flux is presented, representing an upper limit for dust deposition over centennial (African margin) to millennial (Mid-Atlantic Ridge) time scales. Model results of Mahowald *et al.* [31] are shown for reference (blue triangles).

thereby precluding the measurement of other variables on these samples. As in the case of the 0.8–51 µm size fraction, only samples from the depth range 900–3000 m were used to determine ^{230}Th-normalized fluxes of the more than 51 µm size fraction (figure 6*b*, open diamonds).

Dust fluxes calculated by ^{230}Th normalization with the 0.8–51 µm size fraction are lower than the fluxes generated by the model of Mahowald *et al.* [31]. The difference is a factor of 5–6 at the easternmost stations and decreases westwards to a factor of 2.5 at the MAR (figure 6*b*), consistent with the fluxes estimated from the average particle settling rate (figure 6*a*). The ^{230}Th-normalized dust fluxes calculated using the more than 51 µm size fraction are systematically greater than for the 0.8–51 µm size class by 30–40% (figure 6*b*).

(g) Sediment traps

Annual fluxes of lithogenic material collected by sediment traps deployed in the ETNA have been compiled from the original publications [75–81]. Fluxes are included only if the duration of

Table 1. Uranium and thorium data for North Atlantic sediments and ^{230}Th-normalized fluxes of lithogenic material, interpreted here to represent the flux of dust. Lithogenic fluxes were calculated assuming a ^{232}Th content of 13 ppm in dust. Notes: An age of 5000 years is assumed for all samples when making decay corrections for unsupported ^{230}Th. For cores sampled at two depths (V30–49 and V30–51K), the average value of lithogenic flux is plotted in figure 8*b*. Sample V25–21 is taken from a large compilation by Bradtmiller *et al.* [86], and included here to distinguish it from other data in that compilation. Other results are unpublished data generated in the senior author's laboratory at the LDEO.

sample ID	latitude	longitude	water depth (m)	^{232}Th (dpm g^{-1})	^{230}Th (dpm g^{-1})	^{238}U (dpm g^{-1})	lithogenic flux (g m^{-2} yr^{-1})
V22–222tw; 3–4 cm	28.93	−43.65	3197	0.247 ± 0.013	10.044 ± 0.164	0.334 ± 0.013	0.63
V23–110tw; 3–4 cm	17.63	−45.87	3746	0.662 ± 0.021	14.860 ± 0.234	0.501 ± 0.015	1.33
V30–49; 4–5 cm	18.43	−21.08	3093	0.832 ± 0.019	5.155 ± 0.088	0.620 ± 0.021	4.00
V30–49; 11–12 cm	18.43	−21.08	3093	0.662 ± 0.018	5.121 ± 0.093	0.838 ± 0.021	3.21
V30–51K; 4–5 cm	19.87	−19.92	3409	1.654 ± 0.038	7.089 ± 0.121	1.173 ± 0.033	6.39
V30–51K; 9–10 cm	19.87	−19.92	3409	1.053 ± 0.025	5.262 ± 0.091	1.975 ± 0.050	5.54
V25–21; 2 cm	26.40	−45.45	3693	0.497 ± 0.008	18.824 ± 0.298	0.333 ± 0.003	0.78

collection was about a year or longer. Locations of the sediment traps are shown in figure 8*a* and the lithogenic fluxes are presented in figure 8*b*. Hemipelagic sediments mixed seawards from the continental margin may contribute to the water-column inventory of lithogenic particles at sites near the coast [68]. We have made no correction for hemipelagic contributions to the sediment trap samples. Consequently, the fluxes used here represent upper limits for the actual deposition of dust. Lithogenic fluxes collected by sediment traps deployed near the margin are about equally distributed above and below the model reference (figure 8*b*). Unfortunately, we could find results for only one sediment trap, deployed by the EUMELI programme [75] at 31.3° W, close to the GA03 section and located well away from margin sources of hemipelagic sediments. There, the lithogenic flux collected by the sediment trap (3.6 g m^{-2} yr^{-1}) is about half the model reference dust deposition two degrees to the east (6.9 g m^{-2} yr^{-1}, figure 8*b*).

(h) ^{230}Th-normalized fluxes in surface sediments

Concentrations of ^{230}Th and ^{232}Th have been measured in surface sediments at a number of locations throughout the ETNA (figure 8*a*), allowing ^{230}Th-normalized lithogenic fluxes to be calculated (equation (3.7)) using ^{232}Th as a tracer of lithogenic material with an assumed ^{232}Th content of 13 ppm [72]. For the most part we take results from the literature [82–86], to which we add previously unpublished results from the senior author's laboratory for four sites, two on the margin and two on the MAR (table 1).

McGee *et al.* [82] used an algorithm based on grain size to distinguish between hemipelagic sources and dust at the two core sites nearest to the coast of Africa. For these cores, we use the corrected dust fraction. No correction for hemipelagic material has been made at the other core sites near the margin, so the measured lithogenic fluxes at those locations represent upper limits for the dust deposition. ^{230}Th-normalized ^{232}Th fluxes at three sites on the MAR (figure 8*a*) are expected to represent dust deposition more reliably than near the continent because the remote locations of these sites limits the amount of lithogenic material that can be delivered by ocean transport. At the two sites nearest the coast [82], the ^{230}Th-normalized fluxes are in good agreement with the reference model. Further out on the margin, near 21° W, as well as on the MAR, the ^{230}Th-normalized lithogenic flux is one-third to one-half the dust deposition of the reference model (figure 8*b*).

4. Discussion

Observational estimates of dust deposition to the Eastern Tropical North Atlantic span more than two orders of magnitude, ranging from an order of magnitude below (derived from the dissolved Al inventory plus acetate leach aerosol solubility, figure 3) to more than an order of magnitude above (dissolved ^{232}Th inventory plus DI leach aerosol solubility, figure 4) the reference model results [31]. Table 2 provides a general summary of all of the methods. We now discuss some of the factors that may contribute to the large range of estimated dust deposition, concluding with the methods that are thought to involve the smallest 'known unknowns'.

(a) Aerosol settling rates

Duce *et al.* [18] recommend that a factor of 3 uncertainty be applied to aerosol settling rates. Baker *et al.* [45] discuss the factors that cause aerosol settling rates to vary with environmental conditions (presented in §3a), and recommend strategies to reduce uncertainties, such as intercomparison of results obtained using different approaches. For example, here we show that dust deposition estimated using an average aerosol bulk settling velocity of 1000 m day^{-1} is consistent with values derived by normalizing surface aerosol Al concentrations to ^{7}Be (figure 2). Aerosol samples on GA03 were collected during the early portion of the seasonal maximum in local dust deposition (§3a), which is consistent with the scatter of shipboard-derived estimates of dust deposition around the annual averages based on aerosol measurements at the Cape Verde Atmospheric Observatory (figure 2). The sample-to-sample variability in our findings illustrates the need to integrate shipboard observations with long-term monitoring, such as by satellites (e.g. [25]), when estimating annual average dust deposition over the ocean using shipboard surface aerosol concentrations.

(b) Dissolved trace metals in the upper water column

Complications associated with rapid fluctuations in dust supply can be overcome by using the upper water-column inventory of a dissolved trace element delivered by dust because the inventory of a trace element reflects its average supply over its residence time in the upper ocean, which ranges between 1 and 4 years for Th [59–61] and up to about 5 years for Al [53]. In addition, strategies that involve dissolved trace elements may have an advantage when used to constrain the supply of biologically available iron (see the next paragraph). As noted in the Introduction (§1), a major factor motivating research on dust deposition to the ocean is the desire to quantify the source of iron and other essential nutrients supplied by dust. The degree to which particulate forms of iron may be biologically available is a topic of active research, but efforts to constrain the supply of biologically available iron generally focus on the fraction that dissolves in seawater. Operationally defined solubility of aerosol-derived iron spans approximately two orders of magnitude [87]. This large range, and the uncertainty about the environmental factors that regulate it, presents a challenge to the successful modelling of iron supply to marine ecosystems [9] even if dust deposition can be established reliably.

The solubility ratio among elemental constituents in aerosols (e.g. Sol_{Fe}/Sol_{Al} or Sol_{Fe}/Sol_{Th}) may vary over a much smaller range than the absolute solubility. If so, then strategies that exploit measured inventories of dissolved trace elements (e.g. Al, Th) in the ocean would offer an advantage when investigating the supply of dissolved iron. Although efforts to exploit this approach show promise [49,61], significant uncertainties associated with these methods require attention.

Factors contributing most to the uncertainty in dust deposition estimated from dissolved metal inventories include: (i) post-depositional transport by ocean dynamics, (ii) solubility, and (iii) the residence time of the dissolved metal and the nature of the processes responsible for removing it. The wide range of solubility estimates derived using different operational approaches is discussed in §§3c and d. Here, we focus on the other factors.

Table 2. Summary of the dust fluxes to the Eastern Tropical North Atlantic derived using a suite of observational strategies, expressed by comparison to dust fluxes generated by the reference model of Mahowald *et al.* [31]. For each approach, the range of results is presented separately for the eastern and western portions of the study area. Notes: DI = deionized water. Time scale refers to the average period over which each strategy integrates dust signals. 'Relative to model' expresses dust deposition from each observational approach as a fraction of the deposition in the reference model. <, ~ and > indicate that the observationally based dust flux is below, approximately equal to, or above the reference model, respectively. n.a. = not available.

		relative to model	
approach	time scale	west	east
aerosol Al concentration and 1000 m day^{-1} aerosol settling rate	days	0.02	0.16 to 3.5
aerosol Al concentration normalized to aerosol ^{7}Be and water-column ^{7}Be inventory	days	0.01 to 0.6	~ to 3.5
dissolved Al inventory, 5-year residence time, aerosol Al solubility from DI leach	5 years	0.5	< to >
dissolved Al inventory, 5-year residence time, aerosol Al solubility from acetate leach	less than 1–5 years	0.09	0.07
dissolved ^{232}Th inventory, ^{230}Th residence time, aerosol Th solubility from DI leach	1–5 years	4 to 50	1 to 23
dissolved ^{232}Th inventory, ^{230}Th residence time, aerosol Th solubility from acetate leach	1–5 years	1 to 5	0.2 to 1.5
^{230}Th-based particle sinking rate multiplied by lithogenic particle concentration	1–3 years	0.24 to 0.35	0.15 to 0.2
^{230}Th-normalized flux of lithogenic minerals in the 0.8–51 µm particle size fraction	1–3 years	0.25 to 0.4	0.13 to 0.2
^{230}Th-normalized flux of lithogenic minerals in the more than 51 µm particle size fraction	approx. 1 year	n.a.	0.25 to 0.3
flux of lithogenic particles collected by sediment traps	1 year	n.a.	0.2 to 1.4
^{230}Th-normalized flux of lithogenic minerals in surface sediments	millennial	0.3 to 0.6	0.25 to 1.2

(i) Advection and mixing

It is important to keep in mind that the mineral dust deposition calculated using an in-water tracer such as Al or Th is recording the addition of that material to each square metre of surface water, which moves and mixes, not to a geographically static region in the manner of dust deposition maps calculated from real or modelled atmospheric aerosol loads. The degree to which values calculated from these different approaches differ will be directly related to the direction and the relative velocity of the surface water advection; however, there is no reliable way to correct for this advection effect because surface waters do not move as a coherent uniform slab but instead mix with the surrounding water as they move. While each of these estimates has its particular value in quantifying atmospheric deposition processes, from an oceanographic perspective the imprint of a dissolved tracer such as Al or Th in surface water is in fact the most relevant parameter for understanding the impact of dust deposition on oceanic biogeochemical processes. Dissolved tracer concentrations can be used, by ratio, to track the addition of other materials from atmospheric aerosols to the surface water, including nutrients and micronutrients such as Fe, the addition of which can exert significant biological effects.

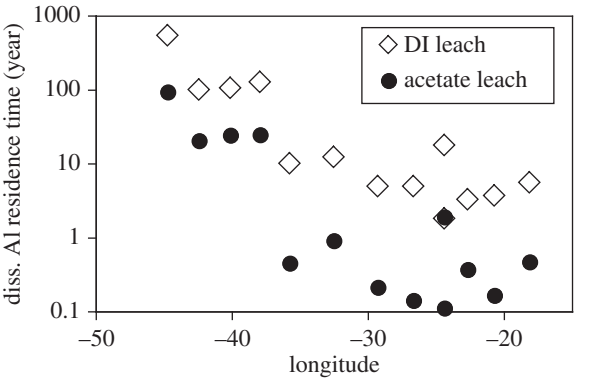

Figure 9. Residence time of dissolved Al in surface waters estimated by dividing the measured dissolved Al inventory in the upper 50 m [50] by the input from aerosols, applying an aerosol settling rate of 1000 m day^{-1} to the measured aerosol Al concentration [37]. Residence times are calculated using results from the application of the instantaneous leach using deionized water [56] and the acetate leach [55] as in figure 3.

In regions where removal of dissolved metals by scavenging occurs at a much faster rate than transport by advection, ocean circulation is expected to contribute little to the overall uncertainty in dust deposition calculated from dissolved metal inventories [45,88]. In highly advective regimes, such as the eastern half of our study area under the influence of the North Equatorial Current [75], the dissolved metal distribution will be spatially smeared to a degree that may be quantifiable as biogeochemical modelling of dissolved trace element cycles improves. Until then we can only have confidence that advection and mixing will tend to reduce spatial gradients imposed by dust deposition, causing an underestimation of dust supply in areas of high deposition and an overestimation in areas of low deposition.

Although models are not yet capable of quantifying the errors introduced by physical redistribution of dissolved metals supplied by dust, as noted above, dust fluxes derived from dissolved Al distributions are generally consistent with estimates based on other methods [13,46–49]. A global analysis by Han *et al.* [89] found that the distribution of surface dissolved Al concentrations is similar to that predicted by dust deposition models. Furthermore, their global compilation of dissolved Al data showed that surface levels are consistent with Al concentrations throughout the water column (fig. 2 of [89]). As surface currents tend to move at much greater velocities than currents below the thermocline [90], this consistency indicates that net lateral transport of dissolved Al by surface currents does not severely decouple surface dissolved Al distributions from dust supply or from the delivery of the dust signal to the deep ocean. Therefore, on a global basis, advective transport is at most a second-order effect, although we do not discount the possibility that it introduces significant uncertainties in regions of strong surface advection.

(ii) Residence time

A critical factor limiting the use of dissolved Al inventories to quantify the supply of dust is the uncertainty of the dissolved Al residence time, including its sensitivity to spatial and temporal variability of biological productivity as well as the abundance and composition of particles that scavenge Al from the water column [45,53,88,89]. To illustrate this point, we calculate the residence time of dissolved Al in surface waters that would be implied by applying an assumed aerosol settling rate of 1000 m day^{-1} to the surface aerosol Al concentration measured along section GA03 (§3a) and multiplying by each set of measured aerosol Al solubility results (§3c). Dividing the measured dissolved Al inventory in the upper 50 m [50] by the dissolved Al supply produces a wide range of residence times (figure 9). If the more aggressive acetate leach reflects the actual solubility of aerosol Al in seawater, then we calculate residence times of much less than

1 year in the eastern portion of our study area (figure 9). Rapid scavenging of dissolved Al in this region is consistent with elevated Al/Ti ratios in particles throughout the water column at stations nearest the African margin [68]. Thus, the rate of scavenging and removal of dissolved Al from surface waters where high particle abundances [67,68] reflect the combined effects of elevated dust flux and biological productivity [57] may be much greater than assumed in calculating the results shown in figure 3. On the other hand, the residence time of dissolved Al in the western portion of our study area may be as large as several decades (figure 9), long enough for substantial redistribution by surface currents.

Another major unknown that limits model-derived estimates of dissolved Al residence time is whether dissolved Al is scavenged primarily by diatoms [88] or if it is removed more uniformly by sorption to all particulate phases [89]. Additional study of the scavenging behaviour of Al is warranted to explore its sensitivity to the abundance and composition of particles and thereby improve the algorithms used to derive dust fluxes from measured dissolved Al inventories.

Thorium has the advantage that its residence time can be calculated from measured U–Th radioactive disequilibrium. However, despite this advantage, exploiting dissolved ^{232}Th as a tracer of aerosol supply presents its own challenges. As noted above, dust deposition calculated from dissolved thorium generally increases with the depth below the surface to which inventories of ^{232}Th and ^{230}Th are integrated (§3d, [60,61]). Future studies will investigate hypotheses that have been proposed to explain this depth dependence. For example, lithogenic particles may continue to dissolve as they settle through the thermocline, perhaps influenced by the biological processes that regenerate most of the organic material exported from the euphotic zone. Alternatively, dust-derived ^{232}Th may be introduced in a colloidal form that reacts differently in seawater than ^{230}Th, which is produced in solution by ^{234}U decay and which is used to determine the residence time of dissolved Th.

Like Al, the use of dissolved Th also suffers from uncertainty about the solubility in seawater of aerosol-derived Th. The better agreement with the reference model obtained using the Th solubility determined with the more aggressive acetate leach (cf. figure 4*a*,*b*) suggests that a substantial fraction of aerosol Th dissolves, consistent with the findings of previous studies [66,91]. If true, then this may indicate that Th is preferentially incorporated into relatively labile phases that coat the surface of dust grains, perhaps formed by weathering in the dust source regions, or that dissolved Th is held in solution through binding by organic ligands, similar to dissolved Fe [92]. These possibilities require further investigation.

(c) Water-column particles and sediments

Net lateral transport of particles in the water column by advection and mixing introduces errors in estimates of dust deposition based on the analysis of solid phases just as it does for approaches applied to dissolved metals. For example, within our study area, Bory *et al.* [75] reported that the flux of particles collected by a deep moored sediment trap at their oligotrophic study site (21° N and 31° W) was correlated with westward current velocity measured at 250 m, from which they inferred that particle fluxes were influenced by westward advection of surface waters as much as 1400 km from the coast of Mauritania. However, the degree to which the measured sinking flux of particles reflected the advective transport of particles versus the biological generation of new particles using dissolved nutrients carried by the North Equatorial Current could not be resolved from their data.

Particles are also redistributed by lateral mixing, even in regions lacking strong surface currents [90,93]. Using results from the Hawaii Ocean Time Series station north of Oahu, Siegel *et al.* [90] calculated that 95% of the particles collected by a moored sediment trap at 4000 m depth originated from a region of surface water having a diameter between 126 and 339 km, for particle sinking rates of 200 and 50 m day^{-1}, respectively, while the mean displacement of particles during transit through the water column is 17 to 54 km. In an earlier study of the region near the Bermuda Time Series station, Siegel & Deuser [93] concluded that the statistical funnel constraining the surface source of 90% of the particles collected by a moored sediment trap at

3200 m is about 300 km, similar to the results from the later study near Hawaii. While these studies demonstrate that deep moored sediment traps cannot resolve strong spatial gradients in surface waters, dispersion of dust particles by lateral mixing in the ocean is not expected to obliterate basin-scale gradients in mean annual dust deposition recorded by deep moored sediment traps or by analysis of dust accumulation in surface sediments.

Next, we consider possible biases in dust fluxes derived from particle settling rates. Ohnemus & Lam [68] estimated the mean settling rate ($m\,yr^{-1}$) of all particles carrying dust by dividing the flux of dust-associated Ti ($\mu g\,m^{-2}\,yr^{-1}$) calculated using results of the AEROCOM median deposition model (see Ohnemus & Lam [68] for details) by the average water-column concentration of total particulate Ti ($\mu g\,m^{-3}$, sum of 0.8–51 µm plus more than 51 µm size fractions). Settling rates obtained using this approach increased from west to east across our study area, from 1825 $m\,yr^{-1}$ at the MAR rising to 5840 $m\,yr^{-1}$ in the region between Africa and the Cape Verde Islands. These settling rates are a factor of 3 (MAR) to 6 (between Cape Verde Islands and Africa) greater than those we derived from the depth dependence of particulate ^{230}Th concentrations using the 0.8–51 µm size fraction, and also show a much larger zonal gradient (figure 5*f*).

In principle, if particles undergo many rounds of aggregation and disaggregation as they settle through the water column, then the chemical composition of the large aggregates should be similar to that of the smaller particles. In this case, the average particle settling rate derived from the depth gradient of the particulate ^{230}Th concentration (equation (3.4)) should be representative of the entire population of particles, even if large aggregates were excluded during the collection of the 0.8–51 µm size fraction that was analysed routinely for Th isotopes. Therefore, if the actual average particle settling rate is three to six times greater than that we infer from the depth gradient of the 0.8–51 µm particulate ^{230}Th concentration, then the implication is that the majority of the large aggregates formed in surface waters must transit the entire water column and reach the sediments without exchanging material with the small size fraction through disaggregation and aggregation.

We can rule out this possibility in the central Atlantic because the dust flux at our westernmost station estimated using the ^{230}Th-based average particle settling rate (0.74 $g\,m^{-2}\,yr^{-1}$, figure 6*a*) falls between the ^{230}Th-normalized lithogenic flux derived from surface sediments collected at the two nearest sites along the MAR (0.63 and 0.86 $g\,m^{-2}\,yr^{-1}$, figure 8*b*). Surface sediments incorporate all size classes and settling rates of particles, so this consistency indicates that applying S_P (equation (3.4), figure 5*f*) to the 0.8–51 µm particle size fraction does not miss a significant fraction of the dust flux.

This possibility can also be ruled out at sites further to the east, where we have analysed a subset of the more than 51 µm size fraction particles. If aggregates sink to the seabed without exchanging material with the small size classes, to which most of the dissolved ^{230}Th is initially adsorbed, then these aggregates would have a deficit of ^{230}Th compared with the smaller particles. Such a deficit would cause us to overestimate the actual dust flux when applying the ^{230}Th-normalization method to the more than 51 µm size fraction because the concentration of ^{230}Th appears in the denominator of the flux calculation (equation (3.7)).

The ^{230}Th-normalized dust flux derived from the more than 51 µm size fraction is, in fact, systematically greater than the flux derived using the 0.8–51 µm size fraction of the same sample (figure 6*b*). This is consistent with some portion of the population of large aggregates settling through the water column without completely exchanging material with the smaller particle size classes. However, the difference is only 30–40% on average (figure 6*b*), much less than the factor of 3–6 difference expected if the bulk average particle settling velocity were as high as estimated by Ohnemus & Lam [68]. Therefore, taking into consideration both the consistency between dust deposition estimated using particle settling rates and ^{230}Th normalization of surface sediment samples near the MAR, and the modest differences between the dust fluxes estimated using large and small particle size classes in the eastern portion of our study area, we conclude that the large aggregates exchange most of their material with smaller size classes as they settle through the

water column. We further suggest that average particle settling rates for this region estimated by Ohnemus & Lam [68] are too large, and return to reconcile the difference at the end of the next section.

(d) Fluxes constrained by normalization to ^{230}Th

Among the approaches described here, we expect the strategies that couple the mass budget of ^{230}Th with the sedimentation and burial of particulate lithogenic phases (§§3e, f and h) to have the smallest uncertainties. Confidence in these approaches rests on the fact that the one-dimensional mass budget of ^{230}Th is known to ±30–40%, as demonstrated in global models [64], in regional models [94] and by applying empirical calculations using dissolved ^{230}Th data from the ETNA [65].

^{230}Th-normalized fluxes of lithogenic material obtained from surface sediments are influenced by two factors that cause overestimation of the historical dust flux. Bioturbation of surface sediments filters the record of sediment accumulation over time scales of centuries (near the continents) to millennia (in the open ocean), so the average fluxes derived from surface sediments include dust supplied by rare large events whose signal in the water column dissipated long ago. Sedimentation on the continental slope and rise may also incorporate episodic input of material that was reworked from sites upslope or on the nearby continental shelf [95], as evidenced by nepheloid layers observed along the African margin [65,68].

Partially offsetting these effects, the preferential scavenging of dissolved ^{230}Th in the particle-rich water column near the coast of Mauritania, combined with lateral mixing, generates a net flux of dissolved ^{230}Th towards the margin. Within the region between Mauritania and Cape Verde Islands, this boundary scavenging effect is estimated to cause the ^{230}Th-normalization approach to underestimate the actual vertical flux of particles by 30–40% [65].

At the two sites nearest the African coast (open red circles in figure 8*b*), the ^{230}Th-normalized lithogenic fluxes derived from surface sediment and corrected for hemipelagic sources [82] are in good agreement with the reference model. Further seawards, near 21° W, ^{230}Th-normalized fluxes of lithogenic material in surface sediments (3.6, 5.6, 5.7 and 6.0 g m^{-2} yr^{-1}) are a factor of 2–3 below the modelled dust deposition at this location (14 g m^{-2} yr^{-1}, figure 8*b*). The 40% error attributable to boundary scavenging in this region is too small to reconcile the difference between the reference model and the ^{230}Th-normalized fluxes. If bioturbation or lateral supply of hemipelagic sediment introduces a significant bias in the ^{230}Th-normalized flux of lithogenic material, which we cannot determine with the available data, then correcting for these factors would amplify the discrepancy between ^{230}Th-normalized fluxes and the reference model.

Results obtained using particles filtered from the water column are consistent with the view that surface sediments near the margin represent upper limits for the historical deposition of dust in this region. Near 21° W, the average ^{230}Th-normalized flux of particulate material collected by *in situ* filtration between 900 m and 3000 m corresponds to a dust flux of 2.3 g m^{-2} yr^{-1} (figure 6*b*). This is a factor of 2 below the ^{230}Th-normalized lithogenic fluxes derived from nearby surface sediments described in the preceding paragraph and, therefore, less than the reference model by a factor of 5–6.

At sites along the MAR (figure 8*a*), far removed from local sources of continental erosion, we expect dust to be the dominant source of lithogenic material. The westernmost hydrographic station within our study area (figure 1) corresponds to the crest of the MAR [36]. There we derive a ^{230}Th-normalized flux of lithogenic particles filtered from the water column of 0.86 g m^{-2} yr^{-1} (figure 6*b*). This falls within the range of ^{230}Th-normalized lithogenic fluxes derived from surface sediments collected at three locations along the MAR (0.63, 0.86 and 1.33 g m^{-2} yr^{-1}, figure 8*b*). These fluxes are about a factor of 2–3 below the reference model dust deposition in this area (2.1 g m^{-2} yr^{-1}).

Methods that couple the well-constrained mass budget of ^{230}Th (±30–40% uncertainty) with the supply and burial of lithogenic particles produce estimates of dust deposition that fall well below the reference model (figures 6*a*,*b* and 8*b*), with the exception of two sites nearest the coast of Africa (open red circles in figure 8*b*). Similarly, a sediment trap deployed at 21° N and 31° W

recorded an annual average flux of lithogenic particles about a factor of 2 below the reference model (figure 8*b*). This trap is located far from lateral reworking of continental margin sediments, but where surface currents may generate a net lateral supply of dust particles originally deposited nearer to Africa [75]. Consequently, if advection of particles by surface currents biases the flux at this site, then we expect the flux collected by the sediment trap to overestimate the actual local dust deposition, further supporting the view that the reference model overestimates the true deposition of dust. Considering that multiple approaches indicate values of dust deposition well below the reference model, we suggest that the model may overestimate dust deposition in this region by a factor of 2–5, with the magnitude of the discrepancy increasing from west to east.

Lowering model dust fluxes accordingly, by a factor of 2 in the west and a factor of 5 in the east, would reconcile the average particle settling velocities described in the preceding section. Dust deposition at our study sites extracted from the AEROCOM median deposition model, as used by Ohnemus & Lam [68], is similar to the deposition estimated by the reference model used here [31], varying between 60% larger at 22.8° W to 7% smaller at 44.8° W (not shown here). Consequently, if the reference model [31] overestimates dust deposition in this region by a factor of 2–5, then this would also be true of the AEROCOM median deposition model. Average particle settling velocities derived by dividing the AEROCOM median model dust (Ti) deposition ($\mu g\,m^{-2}\,yr^{-1}$) by the average measured water-column Ti concentrations ($\mu g\,m^{-3}$) range between 1825 and 5840 $m\,yr^{-1}$ [68], exceeding the settling velocities estimated from the depth dependence of particulate ^{230}Th concentration (660–980 $m\,yr^{-1}$; figure 5) by a factor of 3–6, with the difference increasing from west to east. Reducing the model-derived dust flux by a factor of 2 near the MAR to a factor of 5 in the eastern portion of our study area essentially eliminates the discrepancy between the average particle settling rates derived using the two approaches. More importantly, for interpreting the biogeochemical cycles of other particulate phases, the average particle settling rate increases from west to east across our study area by only a little more than 30% (figure 5*f*) rather than by a factor of 3 [68].

5. Summary and outlook

Each of the strategies to quantify dust deposition discussed in this paper is based on established geochemical principles. However, it is clear from the large range of estimated dust fluxes (figures 2–6 and 8; table 2) that further work is needed to reduce the uncertainties associated with each method before it can be applied routinely to map dust fluxes over the ocean or provide a basis for testing and improving global dust models and satellite retrieval algorithms.

One of the goals that motivated the creation of the GEOTRACES programme was the desire to coordinate research on the processes that supply and remove trace elements in the ocean using multiple tracers and strategies. This study was developed with that goal in mind. Production of a robust (validated) estimate of dust deposition in the Eastern Tropical North Atlantic remains beyond our reach because each of the observational approaches employed here involves substantial uncertainty. Nevertheless, we believe that this synthesis effort has moved us towards the goal of more reliable estimates of dust deposition by identifying inconsistencies among different methods that serve as targets for future research. We contend that this approach would bear fruitful results in other situations also. In this spirit, we encourage readers to consider site-specific factors other than dust deposition that may influence each of the tracers described here, and develop new hypotheses that can be tested using the wealth of data becoming available through the GEOTRACES programme. Doing so will lead to more complete and accurate knowledge of the biogeochemical cycles of trace elements and their isotopes while simultaneously leading to more accurate estimates of dust deposition to the ocean.

Data accessibility. Data from the GEOTRACES programme used in this paper are archived at BCO-DMO in the USA (http://www.bco-dmo.org/project/2066) and at the GEOTRACES Data Assembly Centre in the UK (http://www.bodc.ac.uk/geotraces/).

Authors' contributions. R.F.A. prepared the first draft of the manuscript using data and ideas contributed by each of the other authors. All authors participated in the editing and revision of the manuscript.

Competing interests. The authors indicate that they have no competing interests.

Funding. Collection and analysis of samples collected along GEOTRACES section GA03 were supported by several grants from the Chemical Oceanography Program of the US National Science Foundation: aerosols (OCE-0929919), particles collected by *in situ* pumps (OCE-0963026), thorium (OCE-0927064, OCE-0926860, OCE-0927757 and OCE-0927754) and dissolved aluminium (OCE-0928741 and OCE-1137812). A portion of this work was performed at the National High Magnetic Field Laboratory, which is supported by National Science Foundation Cooperative Agreement No. DMR-1157490 and the State of Florida. L.F.R. was supported by the European Research Council.

Acknowledgements. Comments by M.-E. Carr and two anonymous referees improved earlier versions of this paper. Joanne Goudreau and Maureen Auro prepared samples at the Woods Hole Oceanographic Institution. Figures 1 and 8*a* were produced using Ocean Data View [96]. Samples from Vema cores for which results are presented in table 1 were provided by the core repository at the Lamont-Doherty Earth Observatory. This is LDEO Contribution Number 8054.

References

1. Boyd PW, Ellwood MJ. 2010 The biogeochemical cycle of iron in the ocean. *Nat. Geosci*. **3**, 675–682. (doi:10.1038/ngeo964)
2. Okin GS *et al.* 2011 Impacts of atmospheric nutrient deposition on marine productivity: roles of nitrogen, phosphorus, and iron. *Glob. Biogeochem. Cycles* **25**, GB2022. (doi:10.1029/2010GB003858)
3. Moore CM *et al.* 2009 Large-scale distribution of Atlantic nitrogen fixation controlled by iron availability. *Nat. Geosci*. **2**, 867–871. (doi:10.1038/ngeo667)
4. Moore CM *et al.* 2013 Processes and patterns of oceanic nutrient limitation. *Nat. Geosci*. **6**, 701–710. (doi:10.1038/ngeo1765)
5. Schlosser C, Klar JK, Wake BD, Snow JT, Honey DJ, Woodward EMS, Lohan MC, Achterberg EP, Moore CM. 2014 Seasonal ITCZ migration dynamically controls the location of the (sub)tropical Atlantic biogeochemical divide. *Proc. Natl Acad. Sci. USA* **111**, 1438–1442. (doi:10.1073/pnas.1318670111)
6. Wu J, Sunda W, Boyle EA, Karl DM. 2000 Phosphate depletion in the Western North Atlantic Ocean. *Science* **289**, 759–762. (doi:10.1126/science.289.5480.759)
7. Moore JK, Doney SC, Glover DM, Fung IY. 2001 Iron cycling and nutrient-limitation patterns in surface waters of the World Ocean. *Deep-Sea Res. Part II Topical Stud. Oceanogr.* **49**, 463–507. (doi:10.1016/S0967-0645(01)00109-6)
8. Falkowski PG, Barber RT, Smetacek V. 1998 Biogeochemical controls and feedbacks on ocean primary production. *Science* **281**, 200–206. (doi:10.1126/science.281.5374.200)
9. Tagliabue A *et al.* 2016 How well do global ocean biogeochemistry models simulate dissolved iron distributions? *Glob. Biogeochem. Cycles* **30**, 149–174. (doi:10.1002/2015GB005289)
10. Millero FJ. 1998 Solubility of Fe(III) in seawater. *Earth Planet. Sci. Lett.* **154**, 323–329. (doi:10.1016/S0012-821X(97)00179-9)
11. Bruland KW, Middag R, Lohan MC. 2014 8.2 – Controls of trace metals in seawater. In *Treatise on geochemistry*, 2nd edn (eds HD Holland, KK Turekian), vol. 8, *The oceans and marine geochemistry* (eds MJ Mottl, H Elderfield), pp. 19–51. Oxford, UK: Elsevier. (doi:10.1016/B978-0-08-095975-7.00602-1)
12. Morel FMM, Price NM. 2003 The biogeochemical cycles of trace metals in the oceans. *Science* **300**, 944–947. (doi:10.1126/science.1083545)
13. Vink S, Measures CI. 2001 The role of dust deposition in determining surface water distributions of Al and Fe in the South West Atlantic. *Deep-Sea Res. Part II Topical Stud. Oceanogr.* **48**, 2787–2809. (doi:10.1016/S0967-0645(01)00018-2)
14. Jickells TD *et al.* 2005 Global iron connections between desert dust, ocean biogeochemistry, and climate. *Science* **308**, 67–71. (doi:10.1126/science.1105959)
15. Ussher SJ, Achterberg EP, Powell C, Baker AR, Jickells TD, Torres R, Worsfold PJ. 2013 Impact of atmospheric deposition on the contrasting iron biogeochemistry of the North and South Atlantic Ocean. *Glob. Biogeochem. Cycles* **27**, 1096–1107. (doi:10.1002/gbc.20056)
16. Duce RA, Tindale NW. 1991 Atmospheric transport of iron and its deposition in the ocean. *Limnol. Oceanogr.* **36**, 1715–1726. (doi:10.4319/lo.1991.36.8.1715)
17. Prospero JM, Landing WM, Schulz M. 2010 African dust deposition to Florida: temporal and spatial variability and comparisons to models. *J. Geophys. Res. Atmos.* **115**, D13304. (doi:10.1029/2009jd012773)

18. Duce RA *et al.* 1991 The atmospheric input of trace species to the world ocean. *Glob. Biogeochem. Cycles* **5**, 193–259. (doi:10.1029/91GB01778)
19. Mahowald NM *et al.* 2009 Atmospheric iron deposition: global distribution, variability, and human perturbations. *Annu. Rev. Mar. Sci.* **1**, 245–278. (doi:10.1146/annurev.marine.010908.163727)
20. Kim D *et al.* 2014 Sources, sinks, and transatlantic transport of North African dust aerosol: a multimodel analysis and comparison with remote sensing data. *J. Geophys. Res. Atmos.* **119**, 6259–6277. (doi:10.1002/2013JD021099)
21. Huneeus N *et al.* 2011 Global dust model intercomparison in AeroCom phase I. *Atmos. Chem. Phys.* **11**, 7781–7816. (doi:10.5194/acp-11-7781-2011)
22. Koffi B *et al.* 2012 Application of the CALIOP layer product to evaluate the vertical distribution of aerosols estimated by global models: AeroCom phase I results. *J. Geophys. Res. Atmos.* **117**, D10201. (doi:10.1029/2011jd016858)
23. Evan AT, Flamant C, Fiedler S, Doherty O. 2014 An analysis of aeolian dust in climate models. *Geophys. Res. Lett.* **41**, 5996–6001. (doi:10.1002/2014GL060545)
24. Kok JF, Albani S, Mahowald NM, Ward DS. 2014 An improved dust emission model—Part 2: evaluation in the community earth system model, with implications for the use of dust source functions. *Atmos. Chem. Phys.* **14**, 13 043–13 061. (doi:10.5194/acp-14-13043-2014)
25. Yu H *et al.* 2015 Quantification of trans-Atlantic dust transport from seven-year (2007–2013) record of CALIPSO lidar measurements. *Remote Sens. Environ.* **159**, 232–249. (doi:10.1016/j.rse.2014.12.010)
26. Wagener T, Guieu C, Losno R, Bonnet S, Mahowald N. 2008 Revisiting atmospheric dust export to the Southern Hemisphere ocean: biogeochemical implications. *Glob. Biogeochem. Cycles* **22**, GB2006. (doi:10.1029/2007GB002984)
27. Kohfeld KE, Harrison SP. 2001 DIRTMAP: the geological record of dust. *Earth Sci. Rev.* **54**, 81–114. (doi:10.1016/S0012-8252(01)00042-3)
28. Winckler G, Anderson RF, Fleisher MQ, McGee D, Mahowald NM. 2008 Covariant glacial–interglacial dust fluxes in the Equatorial Pacific and Antarctica. *Science* **320**, 93–96. (doi:10.1126/science.1150595)
29. Henderson GM *et al.* 2007 GEOTRACES—an international study of the global marine biogeochemical cycles of trace elements and their isotopes. *Chem. Erde—Geochem.* **67**, 85–131. (doi:10.1016/j.chemer.2007.02.001)
30. Anderson RF, Mawji E, Cutter GA, Measures CI, Jeandel C. 2014 GEOTRACES: changing the way we explore ocean chemistry. *Oceanography* **27**, 50–61. (doi:10.5670/oceanog.2014.07)
31. Mahowald NM, Baker AR, Bergametti G, Brooks N, Duce RA, Jickells TD, Kubilay N, Prospero JM, Tegen I. 2005 Atmospheric global dust cycle and iron inputs to the ocean. *Glob. Biogeochem. Cycles* **19**, GB4025. (doi:10.1029/2004GB002402)
32. Kallos G, Papadopoulos A, Katsafados P, Nickovic S. 2006 Transatlantic Saharan dust transport: model simulation and results. *J. Geophys. Res. Atmos.* **111**, D09204. (doi:10.1029/2005JD006207)
33. Fomba KW, Mueller K, van Pinxteren D, Poulain L, van Pinxteren M, Herrmann H. 2014 Long-term chemical characterization of tropical and marine aerosols at the Cape Verde Atmospheric Observatory (CVAO) from 2007 to 2011. *Atmos. Chem. Phys.* **14**, 8883–8904. (doi:10.5194/acp-14-8883-2014)
34. Baker AR, Adams C, Bell TG, Jickells TD, Ganzeveld L. 2013 Estimation of atmospheric nutrient inputs to the Atlantic Ocean from 50°N to 50°S based on large-scale field sampling: iron and other dust-associated elements. *Glob. Biogeochem. Cycles* **27**, 755–767. (doi:10.1002/gbc.20062)
35. Powell CF, Baker AR, Jickells TD, Bange HW, Chance RJ, Yodle C. 2015 Estimation of the atmospheric flux of nutrients and trace metals to the eastern tropical north Atlantic Ocean. *J. Atmos. Sci.* **72**, 4029–4045. (doi:10.1175/JAS-D-15-0011.1)
36. Boyle EA, Anderson RF, Cutter GA, Fine R, Jenkins WJ, Saito M. 2015 Introduction to the U.S. GEOTRACES North Atlantic Transect (GA-03): USGT10 and USGT11 cruises. *Deep-Sea Res. Part II Topical Stud. Oceanogr.* **116**, 1–5. (doi:10.1016/j.dsr2.2015.02.031)
37. Shelley RU, Morton PL, Landing WM. 2015 Elemental ratios and enrichment factors in aerosols from the US-GEOTRACES North Atlantic transects. *Deep-Sea Res. Part II Topical Stud. Oceanogr.* **116**, 262–272. (doi:10.1016/j.dsr2.2014.12.005)

38. Taylor SR, McLennan SM. 1995 The geochemical evolution of the continental crust. *Rev. Geophys.* **33**, 241–265. (doi:10.1029/95RG00262)
39. Stuut JB, Zabel M, Ratmeyer V, Helmke P, Schefuss E, Lavik G, Schneider R. 2005 Provenance of present-day eolian dust collected off NW Africa. *J. Geophys. Res. Atmos.* **110**, D04202. (doi:10.1029/2004jd005161)
40. Patey MD, Achterberg EP, Rijkenberg MJ, Pearce R. 2015 Aerosol time-series measurements over the tropical Northeast Atlantic Ocean: dust sources, elemental composition and mineralogy. *Mar. Chem.* **174**, 103–119. (doi:10.1016/j.marchem.2015.06.004)
41. Young JA, Silker WB. 1980 Aerosol deposition velocities on the Atlantic and Pacific Oceans calculated from ^{7}Be measurements. *Earth Planet. Sci. Lett.* **50**, 92–104. (doi:10.1016/0012-821X(80)90121-1)
42. Kadko D, Landing WM, Shelley RU. 2015 A novel tracer technique to quantify the atmospheric flux of trace elements to remote ocean regions. *J. Geophys. Res. Oceans* **120**, 848–858. (doi:10.1002/2014JC010314)
43. Anderson RF, Lao Y, Broecker WS, Trumbore SE, Hofmann HJ, Wolfli W. 1990 Boundary scavenging in the Pacific Ocean—a comparison of ^{10}Be and ^{231}Pa. *Earth Planet. Sci. Lett.* **96**, 287–304. (doi:10.1016/0012-821X(90)90008-L)
44. Kadko D, Johns W. 2011 Inferring upwelling rates in the equatorial Atlantic using ^{7}Be measurements in the upper ocean. *Deep Sea Res. Part I: Oceanogr. Res. Papers* **58**, 647–657. (doi:10.1016/j.dsr.2011.03.004)
45. Baker AR *et al.* 2016 Trace element and isotope deposition across the air–sea interface: progress and research needs. *Phil. Trans. R. Soc. A* **374**, 20160190. (doi:10.1098/rsta.2016.0190)
46. Measures CI, Brown ET. 1996 Estimating dust input to the Atlantic Ocean using surface water aluminium concentrations. In *Impact of desert dust across the Mediterranean* (eds S Guerzoni, R Chester), pp. 301–311. Dordrecht, The Netherlands: Kluwer Academic.
47. Measures CI, Vink S. 2000 On the use of dissolved aluminum in surface waters to estimate dust deposition to the ocean. *Glob. Biogeochem. Cycles* **14**, 317–327. (doi:10.1029/1999GB001188)
48. Measures CI, Brown MT, Vink S. 2005 Dust deposition to the surface waters of the western and central North Pacific inferred from surface water dissolved aluminum concentrations. *Geochem. Geophys. Geosyst.* **6**, Q09M03. (doi:10.1029/2005GC000922)
49. Measures CI, Landing WM, Brown MT, Buck CS. 2008 High-resolution Al and Fe data from the Atlantic Ocean CLIVAR-CO_2 Repeat Hydrography A16N transect: extensive linkages between atmospheric dust and upper ocean geochemistry. *Glob. Biogeochem. Cycles* **22**, GB1005. (doi:10.1029/2007GB003042)
50. Measures C, Hatta M, Fitzsimmons J, Morton P. 2015 Dissolved Al in the zonal N Atlantic section of the US GEOTRACES 2010/2011 cruises and the importance of hydrothermal inputs. *Deep-Sea Res. Part II Topical Stud. Oceanogr.* **116**, 176–186. (doi:10.1016/j.dsr2.2014.07.006)
51. Baker AR, Croot PL. 2010 Atmospheric and marine controls on aerosol iron solubility in seawater. *Mar. Chem.* **120**, 4–13. (doi:10.1016/j.marchem.2008.09.003)
52. Measures CI, Sato T, Vink S, Howell S, Li YH. 2010 The fractional solubility of aluminium from mineral aerosols collected in Hawaii and implications for atmospheric deposition of biogeochemically important trace elements. *Mar. Chem.* **120**, 144–153. (doi:10.1016/j.marchem.2009.01.014)
53. Orians KJ, Bruland KW. 1986 The biogeochemistry of aluminum in the Pacific Ocean. *Earth Planet. Sci. Lett.* **78**, 397–410. (doi:10.1016/0012-821X(86)90006-3)
54. Shelley *et al.* In preparation.
55. Berger CJM, Lippiatt SM, Lawrence MG, Bruland KW. 2008 Application of a chemical leach technique for estimating labile particulate aluminum, iron, and manganese in the Columbia River plume and coastal waters off Oregon and Washington. *J. Geophys. Res.* **113**, C00B01. (doi:10.1029/2007JC004703)
56. Buck CS, Landing WM, Resing JA, Lebon GT. 2006 Aerosol iron and aluminum solubility in the northwest Pacific Ocean: results from the 2002 IOC cruise. *Geochem. Geophys. Geosyst.* **7**, Q04M07. (doi:10.1029/2005GC000977)
57. Carr ME, Kearns EJ. 2003 Production regimes in four Eastern Boundary Current systems. *Deep-Sea Research Part II Topical Stud. Oceanogr.* **50**, 3199–3221. (doi:10.1016/j.dsr2.2003.07.015)
58. Hirose K, Sugimura Y. 1987 Thorium isotopes in the surface air of the western North Pacific Ocean. *J. Environ. Radioact.* **5**, 459–475. (doi:10.1016/0265-931X(87)90020-8)

59. Hsieh Y-T, Henderson GM, Thomas AL. 2011 Combining seawater ^{232}Th and ^{230}Th concentrations to determine dust fluxes to the surface ocean. *Earth Planet. Sci. Lett.* **312**, 280–290. (doi:10.1016/j.epsl.2011.10.022)
60. Hayes CT, Anderson RF, Fleisher MQ, Serno S, Winckler G, Gersonde R. 2013 Quantifying lithogenic inputs to the North Pacific Ocean using the long-lived thorium isotopes. *Earth Planet. Sci. Lett.* **383**, 16–25. (doi:10.1016/j.epsl.2013.09.025)
61. Hayes CT, Fitzsimmons JN, Boyle EA, McGee D, Anderson RF, Weisend R, Morton PL. 2015 Thorium isotopes tracing the iron cycle at the Hawaii Ocean Time-series Station ALOHA. *Geochim. Cosmochim. Acta* **169**, 1–16. (doi:10.1016/j.gca.2015.07.019)
62. Deng F, Thomas AL, Rijkenberg MJA, Henderson GM. 2014 Controls on seawater ^{231}Pa, ^{230}Th and ^{232}Th concentrations along the flow paths of deep waters in the Southwest Atlantic. *Earth Planet. Sci. Lett.* **390**, 93–102. (doi:10.1016/j.epsl.2013.12.038)
63. Bacon MP, Anderson RF. 1982 Distribution of thorium isotopes between dissolved and particulate forms in the deep-sea. *J. Geophys Res. Oceans Atmos.* **87**, 2045–2056. (doi:10.1029/JC087iC03p02045)
64. Henderson GM, Heinze C, Anderson RF, Winguth AME. 1999 Global distribution of the ^{230}Th flux to ocean sediments constrained by GCM modelling. *Deep-Sea Res. Part I Oceanogr. Res. Papers* **46**, 1861–1893. (doi:10.1016/S0967-0637(99)00030-8)
65. Hayes CT, Anderson RF, Fleisher MQ, Huang K-F, Robinson LF, Lu Y, Cheng H, Edwards RL, Moran SB. 2015 ^{230}Th and ^{231}Pa on GEOTRACES GA03, the U.S. GEOTRACES North Atlantic transect, and implications for modern and paleoceanographic chemical fluxes. *Deep-Sea Res. Part II Topical Stud. Oceanogr.* **116**, 29–41. (doi:10.1016/j.dsr2.2014.07.007)
66. Hayes CT *et al.* 2015 Intensity of Th and Pa scavenging partitioned by particle chemistry in the North Atlantic Ocean. *Mar. Chem.* **170**, 49–60. (doi:10.1016/j.marchem.2015.01.006)
67. Lam PJ, Ohnemus DC, Auro ME. 2015 Size-fractionated major particle composition and concentrations from the US GEOTRACES North Atlantic Zonal Transect. *Deep-Sea Res. Part II Topical Stud. Oceanogr.* **116**, 303–320. (doi:10.1016/j.dsr2.2014.11.020)
68. Ohnemus DC, Lam PJ. 2015 Cycling of lithogenic marine particles in the US GEOTRACES North Atlantic transect. *Deep-Sea Res. Part II Topical Stud. Oceanogr.* **116**, 283–302. (doi:10.1016/j.dsr2.2014.11.019)
69. Krishnaswami S, Lal D, Somayajulu BLK, Weiss RF, Craig H. 1976 Large volume *in situ* filtration of deep Pacific waters: mineralogical and radioisotope studies. *Earth Planet. Sci. Lett.* **32**, 420–429. (doi:10.1016/0012-821X(76)90082-0)
70. Berelson W. 2001 Particle settling rates increase with depth in the ocean. *Deep-Sea Res. Part II Topical Stud. Oceanogr.* **49**, 237–251. (doi:10.1016/S0967-0645(01)00102-3)
71. Bacon MP, Huh CA, Fleer AP, Deuser WG. 1985 Seasonality in the flux of natural radionuclides and plutonium in the deep Sargasso Sea. *Deep-Sea Res. Part A Oceanogr. Res. Papers* **32**, 273–286. (doi:10.1016/0198-0149(85)90079-2)
72. Muhs DR, Budahn JR, Prospero JM, Carey SN. 2007 Geochemical evidence for African dust inputs to soils of western Atlantic islands: Barbados, the Bahamas, and Florida. *J. Geophys. Res. Earth Surf.* **112**, F02009. (doi:10.1029/2005JF000445)
73. Francois R, Frank M, Rutgers van der Loeff MM, Bacon MP. 2004 ^{230}Th normalization: an essential tool for interpreting sedimentary fluxes during the late Quaternary. *Paleoceanography* **19**, PA1018. (doi:10.1029/2003PA000939)
74. Anderson RF, Fleisher MQ, Lao Y. 2006 Glacial–Interglacial variability in the delivery of dust to the central equatorial Pacific Ocean. *Earth Planet. Sci. Lett.* **242**, 406–414. (doi:10.1016/j.epsl.2005.11.061)
75. Bory A *et al.* 2001 Downward particle fluxes within different productivity regimes off the Mauritanian upwelling zone (EUMELI program). *Deep-Sea Res. Part A Oceanogr. Res. Papers* **48**, 2251–2282. (doi:10.1016/S0967-0637(01)00010-3)
76. Nowald N, Iversen MH, Fischer G, Ratmeyer V, Wefer G. 2015 Time series of *in-situ* particle properties and sediment trap fluxes in the coastal upwelling filament off Cape Blanc, Mauritania. *Progr. Oceanogr.* **137**, 1–11. (doi:10.1016/j.pocean.2014.12.015)
77. Helmke P, Romero O, Fischer G. 2005 Northwest African upwelling and its effect on offshore organic carbon export to the deep sea. *Glob. Biogeochem. Cycles* **19**, GB4015. (doi:10.1029/2004GB002265)

78. Fischer G *et al.* 2009 Mineral ballast and particle settling rates in the coastal upwelling system off NW Africa and the South Atlantic. *Int. J. Earth Sci.* **98**, 281–298. (doi:10.1007/s00531-007-0234-7)
79. Quiñones RA *et al.* 2010 Eastern boundary current systems. In *Carbon and nutrient fluxes in continental margins* (ed. KK Liu), pp. 25–120. Heidelberg, Germany: Springer.
80. Ratmeyer V, Balzer W, Bergametti G, Chiapello I, Fischer G, Wyputta U. 1999 Seasonal impact of mineral dust on deep-ocean particle flux in the eastern subtropical Atlantic Ocean. *Mar. Geol.* **159**, 241–252. (doi:10.1016/S0025-3227(98)00197-2)
81. Ratmeyer V, Fischer G, Wefer G. 1999 Lithogenic particle fluxes and grain size distributions in the deep ocean off northwest Africa: implications for seasonal changes of aeolian dust input and downward transport. *Deep-Sea Res. Part A Oceanogr. Res. Papers* **46**, 1289–1337. (doi:10.1016/S0967-0637(99)00008-4)
82. McGee D, deMenocal PB, Winckler G, Stuut JBW, Bradtmiller LI. 2013 The magnitude, timing and abruptness of changes in North African dust deposition over the last 20 000 yr. *Earth Planet. Sci. Lett.* **371–372**, 163–176. (doi:10.1016/j.epsl.2013.03.054)
83. Legeleux F, Reyss JL, Schmidt S. 1994 Particle mixing rates in sediments of the northeast tropical Atlantic—evidence from $^{210}Pb_{xs}$, ^{137}Cs, $^{228}Th_{xs}$ and $^{234}Th_{xs}$ downcore distributions. *Earth Planet. Sci. Lett.* **128**, 545–562. (doi:10.1016/0012-821X(94)90169-4)
84. Legeleux F, Reyss JL, Floris S. 1995 Trace metal removal to sediments on the eastern Atlantic continental margins. *C. R. Acad. Sci. Ser. II Sci. Terre Planetes* **320**, 1195–1202.
85. Meckler AN *et al.* 2013 Deglacial pulses of deep-ocean silicate into the subtropical North Atlantic Ocean. *Nature* **495**, 495–498. (doi:10.1038/nature12006)
86. Bradtmiller LI, McManus JF, Robinson LF. 2014 $^{231}Pa/^{230}Th$ evidence for a weakened but persistent Atlantic meridional overturning circulation during Heinrich Stadial 1. *Nat. Commun.* **5**, 5817. (doi:10.1038/ncomms6817)
87. Sholkovitz ER, Sedwick PN, Church TM, Baker AR, Powell CF. 2012 Fractional solubility of aerosol iron: synthesis of a global-scale data set. *Geochim. Cosmochim. Acta* **89**, 173–189. (doi:10.1016/j.gca.2012.04.022)
88. van Hulten MMP, Sterl A, Tagliabue A, Dutay JC, Gehlen M, de Baar HJW, Middag R. 2013 Aluminium in an ocean general circulation model compared with the West Atlantic GEOTRACES cruises. *J. Mar. Syst.* **126**, 3–23. (doi:10.1016/j.jmarsys.2012.05.005)
89. Han Q, Moore JK, Zender C, Measures C, Hydes D. 2008 Constraining oceanic dust deposition using surface ocean dissolved Al. *Glob. Biogeochem. Cycles* **22**, GB2003. (doi:10.1029/2007GB002975)
90. Siegel DA, Fields E, Buesseler KO. 2008 A bottom-up view of the biological pump: modeling source funnels above ocean sediment traps. *Deep-Sea Res. Part I Oceanogr. Res. Papers* **55**, 108–127. (doi:10.1016/j.dsr.2007.10.006)
91. Robinson LF, Noble TL, McManus JF. 2008 Measurement of adsorbed and total $^{232}Th/^{230}Th$ ratios from marine sediments. *Chem. Geol.* **252**, 169–179. (doi:10.1016/j.chemgeo.2008.02.015)
92. Barbeau K, Kujawinski EB, Moffett JW. 2001 Remineralization and recycling of iron, thorium and organic carbon by heterotrophic marine protists in culture. *Aquat. Microb. Ecol.* **24**, 69–81. (doi:10.3354/ame024069)
93. Siegel DA, Deuser WG. 1997 Trajectories of sinking particles in the Sargasso Sea: modeling of statistical funnels above deep-ocean sediment traps. *Deep-Sea Res. Part I Oceanogr. Res. Papers* **44**, 1519–1541. (doi:10.1016/S0967-0637(97)00028-9)
94. Siddall M, Anderson RF, Winckler G, Henderson GM, Bradtmiller LI, McGee D, Franzese A, Stocker TF, Muller SA. 2008 Modeling the particle flux effect on distribution of ^{230}Th in the equatorial Pacific. *Paleoceanography* **23**, PA2208. (doi:10.1029/2007PA001556)
95. Biscaye PE, Anderson RF. 1994 Fluxes of particulate matter on the slope of the southern Middle Atlantic Bight—SEEP-II. *Deep-Sea Res. Part II Topical Stud. Oceanogr.* **41**, 459–509. (doi:10.1016/0967-0645(94)90032-9)
96. Schlitzer R. 2013 Ocean Data View. See http://odv.awi.de/.